Song, L., Guanter, L., Guan, K., You, L., Huete, A., Ju, W., Zhang, Y. (2018): Satellite sun-induced chlorophyll fluorescence detects early response of winter wheat to heat stress in the Indian Indo-Gangetic Plains. - *Global Change Biology*, *24*, 9, pp. 4023—4037.

DOI: http://doi.org/10.1111/gcb.14302

**Title: Satellite sun-induced chlorophyll fluorescence detects early response of winter wheat to heat stress in the Indian Indo-Gangetic Plains**

Lian Song[1, 2], Luis Guanter[3], Kaiyu Guan[4], Liangzhi You[5, 6], Alfredo Huete[7], Weimin Ju[1, 2], Yongguang Zhang[1, 2*]

[1] *International Institute for Earth System Sciences, Nanjing University, 210023 Nanjing, China*

[2] *Jiangsu Center for Collaborative Innovation in Geographical Information Resource Development and Application, 210023 Nanjing, China;*

[3] *Helmholtz Center Potsdam, GFZ German Research Center for Geosciences, Remote Sensing Section, Telegrafenberg A17, 14473 Potsdam, Germany;*

[4] *Department of Natural Resources and Environmental Sciences and National Center for Supercomputing Applications, University of Illinois at Urbana Champaign, Illinois, USA;*

[5] *College of Plant Science &Technology, Huazhong Agricultural University, 430070 Wuhan, China*

[6] *International Food Policy Research Institute, 1201 Eye Street, NW, Washington, DC, USA;*

[7] *Plant Functional Biology and Climate Change Cluster, University of Technology Sydney, NSW 2007, Australia;*

* Corresponding author, phone: +86-2589681569,
E-mail: yongguang.zhang@nju.edu.cn

## Abstract

Extremely high temperatures represent one of the most severe abiotic stresses limiting crop productivity. However, understanding crop responses to heat stress is still limited considering the increases in both the frequency and severity of heat wave events under climate change. This limited understanding is partly due to the lack of studies or tools for the timely and accurate monitoring of crop responses to extreme heat over broad spatial scales. In this work, we use novel space-borne data of sun-induced chlorophyll fluorescence (SIF), which is a new proxy for photosynthetic activity, along with traditional vegetation indices (Normalized Difference Vegetation Index NDVI & Enhanced Vegetation Index EVI) to investigate the impacts of heat stress on winter wheat in northwestern India, one of the world's major wheat production areas. In 2010, an abrupt rise in temperature that began in March adversely affected the productivity of wheat and caused yield losses of 6% compared to previous year. The yield predicted by satellite observations of SIF decreased by approximately 13.9%, compared to the 1.2% and 0.4% changes in NDVI and EVI respectively. During early stage of this heat wave event in early March 2010, the SIF observations showed a significant reduction and earlier response, while NDVI and EVI showed no changes and could not capture the heat stress until late March. The spatial patterns of SIF anomalies closely tracked the temporal evolution of the heat stress over the study area. Furthermore, our results show that SIF can provide large-scale physiology-related wheat stress response as indicated by the larger reduction in fluorescence yield ($SIF_{yield}$) than fraction of

Photosynthetically Active Radiation during the grain-filling phase, which may have eventually led to the reduction in wheat yield in 2010. This study implies that satellite observations of SIF have great potential to detect heat stress conditions in wheat in a timely manner and assess their impacts on wheat yields at large scales.

**Keywords:** Heat stress, Crop yield, Sun-induced chlorophyll fluorescence, Extreme climatic events, Winter wheat

## 1. Introduction

Wheat is the third largest crop in the world with production at 735 million metric tons (MMT) in 2017-18 and plays an essential role in global food security (Bryant-Erdmann 2017). There is extensive evidence that both the mean and variability of temperature have increased globally over the past several decades, including the major wheat producing regions (Hennessy et al. 2008); this trend will continue and may be reinforced (Field 2012). Especially in India, the temperatures are predicted to increase by 2 to 4 ℃ by 2050 (IPCC 2014; Rohini et al. 2016). When wheat experiences extremely high temperatures, in particular during the key growing stages such as grain-filling, severe cellular injury and cell death will occur within minutes, which will result in a decline in the yield (Schöffl et al. 1999).

It is essential to understand the mechanisms of high-temperature impacts on wheat yields and monitor its influence across space and time. Crop simulation models are generally used to investigate such influences, because they can simulate several important crop physiological processes under various climatic variations (Challinor et al. 2005; Asseng et al. 2013; Koehler et al. 2013). Many models have considered the effects of temperature on crop development and grain-filling rates. However, these models may not accurately account for extreme temperatures well (White 2003). For example, the Agricultural Production Systems Simulator (APSIM) model considers the impacts of high temperatures greater than 34 ℃ on the acceleration of crop senescence (Asseng et al. 2011). However, the APSIM model still overestimated length of the wheat growing season in warming temperatures and resulted in the underestimation of wheat yield losses due to the 2010 heat stress in the Indo-Gangetic Plains (IGP) of India (Lobell et al. 2012).

Satellite observations of vegetation status provide a unique opportunity to quantify the impacts of high temperatures on crops. Traditional vegetation indices such as the Normalized Difference Vegetation Index (NDVI) and Enhanced Vegetation Index (EVI) are generally used to evaluate crop conditions (Verhulst et al. 2011), and predict crops yield (Labus et al. 2002; Quarmby et al. 1993). Some vegetation indices (VIs) such as the photochemical reflectance index (PRI) that captures the xanthophyll cycle link the status of the epoxidation of xanthophyll pigments and monitor the changes in plant pigments due to changes in photosynthetic light use efficiency (Gamon et al. 1990; Gamon et al. 1992; Gamon et al. 1997; Barton et al. 2001; Magney et al. 2016). However, VIs may not be able to detect the rapid changes in the photosynthetic functioning of vegetation induced by climate stress such as heat stress. (Dobrowski et al. 2005).

Recent satellite observations of sun-induced chlorophyll fluorescence (SIF) provide novel measurements to monitor crop growth conditions and stress responses, which may complement existing VIs. When photosynthetically active radiation (PAR) is absorbed by a leaf, it can undergo one of three pathways: drive photochemical reactions, lost through regulated non-photochemical quenching (NPQ) or remitted at longer wavelengths as fluorescence (Baker 2008). SIF contains information about the biochemical, physiological and metabolic functions of a plant and the amount of absorbed PAR (APAR) (Porcar-Castell et al. 2014). Many leaf-level studies have demonstrated that chlorophyll fluorescence has a direct relationship with the actual photosynthesis in plants and can respond rapidly when plants are under environmental stress (Chappelle et al. 1984; Chappelle et al. 1985; Moya et al. 2004). Global SIF products have been recently retrieved from several space-borne instruments such as SCIAMACHY (Joiner et al. 2012), GOME-2 (Köhler et al. 2015; Joiner et al. 2013), GOSAT (Köhler et al. 2015; Guanter et al. 2012; Frankenberg et al. 2011) and OCO-2 (Frankenberg et al. 2014). These satellite SIF products make it possible to study vegetation photosynthetic activities at large scales. Many studies have demonstrated that satellite SIF is more sensitive to the photosynthetic rates of plants than other remotely sensed vegetation parameters (Zhang et al. 2014; Guanter et al. 2014) and it is highly correlated with the gross primary production (GPP) of crops (Wagle et al. 2015; Verma et al. 2017; Sun et al. 2017). In terms of plant stress responses, space-borne SIF has also been proved to have high sensitivity to water stress, heat stress and drought monitoring (Lee et al. 2013; Sun et al. 2015; Guan et al. 2016; Yoshida et al. 2015).

We hypothesize that SIF is more sensitive to heat stress events for crops than traditional VIs because it has a physiological link to photosynthesis. To test this hypothesis we conduct a study in the wheat growing region in the IGP of India. Our study area includes the wheat growing regions in Punjab, Haryana and Uttar Pradesh in the IGP of India. In India, wheat is grown over an area of approximately 30 million ha, which is primarily concentrated in the Punjab-Haryana belt, thus IGP has been regarded as the bread basket of India (Swaminathan et al. 2013). In 2010, during the wheat grain filling and harvesting stages (March and April), an abrupt rise in temperature in this region caused a significant decline in the wheat yield (Gupta et al. 2010). Thanks to the development of irrigation infrastructure, more than 90% of wheat was irrigated and received normal precipitation (Duncan et al. 2015). Hence, water conditions are not the limiting factors for wheat yield (Gupta et al. 2007; Erenstein 2009). The previously described situations make the 2010 heat stress in the IGP wheat belt as an ideal case to use satellite SIF to study the influence of heat stress on winter wheat.

In this work, we will explore the potential of utilizing satellite observations of SIF to assess the impacts of heat stress on winter wheat in the IGP of India, with a special focus on the 2010 heat wave event. Specifically we aim to address the following questions: 1) To what extent can SIF capture the heat stress in winter wheat? 2) Compared with traditional VIs, does SIF show an advantage for heat stress detection (e.g. earlier detection, or better capture of yield losses) in wheat? 3) Can SIF serve as an effective indicator to predict winter wheat yields?

## 2. MATERIALS AND METHODS

### *2.1 Study area*

The study area is located in north-west India in the IGP (Figure 1). The soils of the study area generally have moderate water-holding capacities, are highly fertile and are underlain by extensive aquifers that profit from an extensive groundwater network for irrigation (Chauhan et al. 2012). The rice-wheat (RW) cropping system has dominated the study area since the Green Revolution. In the IGP, wheat is usually grown in the dry winter season (November-December to March-April) and rice is grown in the wet summer season (May-June to October-November) (Pathak et al. 2003). The entire study region includes three states: Punjab, Haryana and Uttar Pradesh. The three states together supply approximately 65% of the wheat output of India (TYAGI et al. 2013).

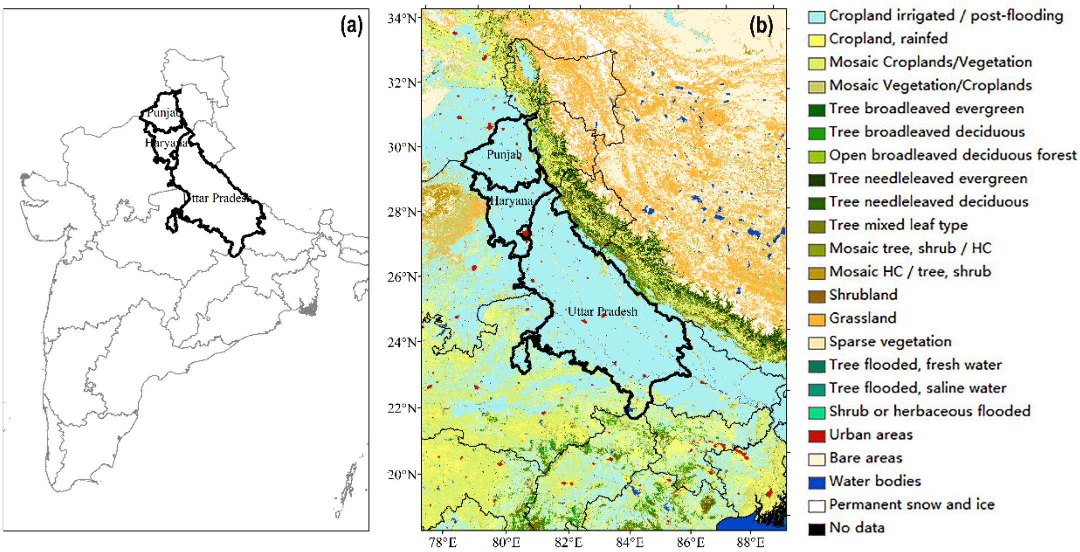


Figure 1. The study area of the Indo-Gangetic Plains in north-west India. (a) The three selected states include Punjab, Haryana and Uttar Pradesh in the study area. (b) The ESA Climate Change Initiative (CCI) land cover map of the study region in 2010 at 300 m spatial resolution.

*2.2 Satellite SIF and vegetation indices*

We used satellite retrievals of SIF from the GOME-2 instrument onboard

EUMETSAT's MetOp-A platform and the Fourier Transform Spectrometer (FTS) onboard the GOSAT platform. The spectral range of GOME-2 is covered by four detector channels between 240 and 790 nm, and the fourth channel ranges from 590 to 790 nm with a spectral resolution of 0.5 nm and a signal-to-noise (SNR) of up to 2000. Based on the previous SIF retrieval algorithms by Guanter et al. (2013) and Joiner et al. (2013), Köhler et al. (2015) used an improved algorithm to retrieve the SIF at 740 nm from a spectral range between 720 and 758 nm, which reduced the retrieval noise and sensitivity of the SIF retrieval to cloud contamination. Specifically, the retrieval method disentangles the contributions of atmospheric absorption and scattering, surface reflectance, and fluorescence to the measured top-of-atmosphere radiance spectra; and more details can be found in (Köhler et al. 2015). The SIF data are quality filtered by removing pixels with solar zenith angles greater than 70° and cloud fractions up to 30%, and then the quality controlled SIF data have been gridded to 0.5° spatial resolution and 16-day and monthly temporal resolutions. We also used the SIF data at 770nm from the Thermal And Near-infrared Sensor for carbon Observation- Fourier Transform Spectrometer (TANSO-FTS) onboard GOSAT which is retrieved from band 1 that extends from approximately 758 to 775nm (Guanter et al. 2012). However, due to the sparse sampling of the GOSAT SIF retrievals, the GOSAT SIF are used as only complements for the GOME-2 SIF data in this study.

The VIs used in this work include the NDVI from the Advanced Very High Resolution Radiometer (AVHRR) instruments and the EVI from the Moderate

Resolution Imaging Spectroradiometer (MODIS). We used the Global Inventory Modelling and Mapping Studies (GIMMS) AVHRR NDVI data (GIMMS 3g v1) with a 1/12° spatial resolution and biweekly temporal resolution from 2007 to 2014. The NDVI data included overall preprocessing steps such as channel calibration, reduction of the effects of the varying solar zenith angle and calibration of the probability density functions (Pinzon et al. 2014). To reduce the effects of cloud cover and aerosol contamination, the AVHRR NDVI data were composited using the highest NDVI value over a two-week composite period. The 16-day MODIS EVI product at 0.05° spatial resolution (MOD13C1 collection 6) was acquired from NASA (http://reverb.echo.nasa.gov/reverb/). The MOD13C1 is the Terra MODIS level 3 vegetation index product, and contains reliability and QA layers. The MODIS EVI data were quality filtered by excluding pixels contaminated by clouds or aerosols using quality flags (Solano et al. 2010).

The fraction of PAR absorbed by vegetation canopies that is derived from the MODIS product (MOD15A2 fPAR collection 6) was used in this work to reveal the SIF dynamics. The MOD15A2 fPAR is a standard 1 km spatial resolution product for EOS-MODIS with an 8-day temporal resolution (Myneni et al. 2002).

### *2.3 Meteorological data*

The air temperature (2 m above the land surface) was obtained from the Climatic Research Unit (CRU) NCEP reanalysis datasets at a daily scale and a 0.5° spatial resolution from 2007 to 2014 (Version

6; http://dods.extra.cea.fr/data/p529viov/cruncep/readme.htm). The CRU-NCEP climate data are a combination of two data sets: the ground observation-based CRU TS 3.2 data and the model-based NCEP-NCAR data at a 6-h temporal resolution. We rescaled the 6 h data to 16-day and monthly temporal scales corresponding to the SIF data.

*2.4 Wheat area and yield*

The annual county-scale wheat yields of the study region were taken from Indiastat (http://www.indiastat.com/default.aspx). We downloaded both district-level and province-level data and further cleaned and validated the data to make them consistent with each other. To identify wheat pixels in the study area, we used the irrigated wheat maps from the Spatial Production Allocation Model (SPAM, http://mapspam.info) and the Land Cover Type Climate Modeling Grid (CMG) product (MCD12C1 version 051) in the International Geosphere-Biosphere Programme (IGBP) land cover type. The SPAM includes the harvest area, production and yield products for 40 crops and three management systems: irrigated, high-input rainfed and low-input rainfed. A variety of inputs and a cross-entropy approach were employed to estimate the crop distribution with a 5-arc-minute spatial resolution (You et al. 2006; You et al. 2014). The MODIS land cover data in the IGBP type identifies 17 land cover classes, which include 11 natural vegetation classes, 3 developed and mosaicked land types and 3 non-vegetated land classes (Friedl et al. 2010). The croplands type was used here to further identify wheat-only pixels.

*2.5 Analysis*

The spatial means of all aforementioned variables were calculated at three spatial scales: the entire study area, the state level and the county level. At the county scale, the spatial mean value was calculated by using the India county boundary to obtain the extents of the counties in the study area. The anomalies were computed as departures from the multiyear means from 2007 to 2014 for all datasets except GOSAT SIF. The GOSAT SIF data are available since 2009, so the anomaly was calculated as the departure from the multiyear mean from 2009 to 2014. The relative changes of all variables were calculated as the anomalies divided by their multiyear mean value. To better compare the spatial dynamics of SIF and NDVI, we calculated their normalized anomalies as follows:

$$\mathrm{Y(i,j,t)}' = \frac{(Y(i,j,t) - \bar{Y}(i,j))}{std(Y(i,j,t))} \qquad (1)$$

where $\mathrm{Y(i,j,t)}'$ denotes the normalized SIF/NDVI anomalies of pixel (i,j) at time t; $Y(i,j,t)$ is the original SIF/NDVI/EVI anomaly value of pixel (i,j) at time t; $\bar{Y}(i,j)$ is the mean anomaly value at (i,j) during 2007-2014, and $std(Y(i,j,t))$ is the standard deviation of the anomalies at (i,j) during 2007-2014.

The inventory-based wheat yield of each county in the study area from 2008 to 2013 was used here as further validation for the SIF, NDVI and EVI. We summed the county-level yield to obtain the yield of the entire study region. To match the spatial and temporal resolution of the aforementioned datasets, we resampled all other variables based on the GOME-2 SIF and then aggregated the SIF and CRUNCEP data into 16-day means, which are consistent with the AVHRR NDVI and MODIS EVI products.

To further explore the difference between SIF and VIs, we interpreted SIF with fPAR and $SIF_{yield}$. The actual amount of SIF at the top of the canopy can be expressed as:

$$\mathrm{SIF} = \mathrm{fPAR} \times \mathrm{PAR} \times \varepsilon_f \times \Omega_c \tag{2}$$

$$\mathrm{SIF} = APAR \times SIF_{yield} \tag{3}$$

where fPAR is the fraction of absorbed PAR, $\varepsilon_f$ is the actual fluorescence yield (defined as the intrinsic light-use efficiency for SIF), and $\Omega_c$ is a term accounting for the fraction of leaf-level SIF photons escaping the canopy. Here, we define $SIF_{yield} = \varepsilon_f \times \Omega_c$ which is the product of the actual fluorescence yield of the canopy and the fractional amount of fluorescence that escapes from the top of canopy. Thus, $SIF_{yield}$ is determined by leaf biochemistry and partly by canopy structure. $\Omega_c$ is usually assumed to be fairly constant for crops with relatively simple canopy structure and high leaf area index, especially when canopy structure is not changing (Guanter et al. 2014; Yoshida et al. 2015). The $SIF_{yield}$ eliminates the effects of APAR on SIF and can be used to indicate photosynthetic efficiency of plants. Under clear-sky conditions of satellite overpass, we can simply attribute the variations in $SIF_{APAR\_norm}$ as the spatial and temporal dynamics of the $SIF_{yield}$ as follows (Sun et al. 2015; Yoshida et al. 2015).

$$SIF_{APAR\_norm} = \frac{SIF}{\cos(SZA) \times fPAR} \tag{4}$$

where *SZA* is the solar zenith angle at the satellite overpass time. $SIF_{APAR\_norm}$ can be considered as *apparent fluorescence yield* which can also be used to account for the changes of plant physiological status.

## 3. Results

### *3.1 Interannual variations in wheat yield and SIF/NDVI/EVI*

We first compare the interannual variations of the wheat yield and the satellite observations of SIF, NDVI and EVI of the entire region during 2008-2013. We find that SIF captures the interannual variations of wheat yield better than NDVI and EVI (Figure 2-a). During 2010, heat stress causes yield losses of approximately 6% compared to yield in the previous year. The SIF- wheat yield regression models indicate that SIF can capture the 2010 yield losses with approximately 13.9% decline compared to that in the year of 2009. However, with nearly 0% changes in the EVI and unexpected an 1.2% increase in the NDVI compared with that in the previous year, VIs show little signal of this yield loss. The phenology results calculated by SIF suggest that this heat stress has significantly shortened the wheat growing season length by approximately 11 days. In contrast, the NDVI data indicate that these results are approximately 2 days (Figure S1).

The relationship between spaceborne SIF and yield is significant and high ($R^2$=0.8, $P<0.05$) at the regional scale (Figure 2-a). This result indicates that satellite observations of SIF can explain approximately 80% of the interannual and spatial variations in wheat grain yields. The $R^2$ between NDVI, EVI and yield are 0.78 and 0.72 respectively, which are slightly lower than that between SIF and yield. The difference between SIF and NDVI/EVI as a proxy for crop yield becomes evident at the county scale (Figure 2-b, c & d). SIF can explain approximately 65% of the interannual and spatial variations in wheat yields, whereas this value is 42% for NDVI and 47% for EVI. NDVI/EVI contain more errors in approximating yield when yield is greater than 4000 Kg/Hectare or less than 2000 Kg/Hectare, as NDVI/EVI tends to underestimate (overestimate) the yield for high (low) yield ranges.

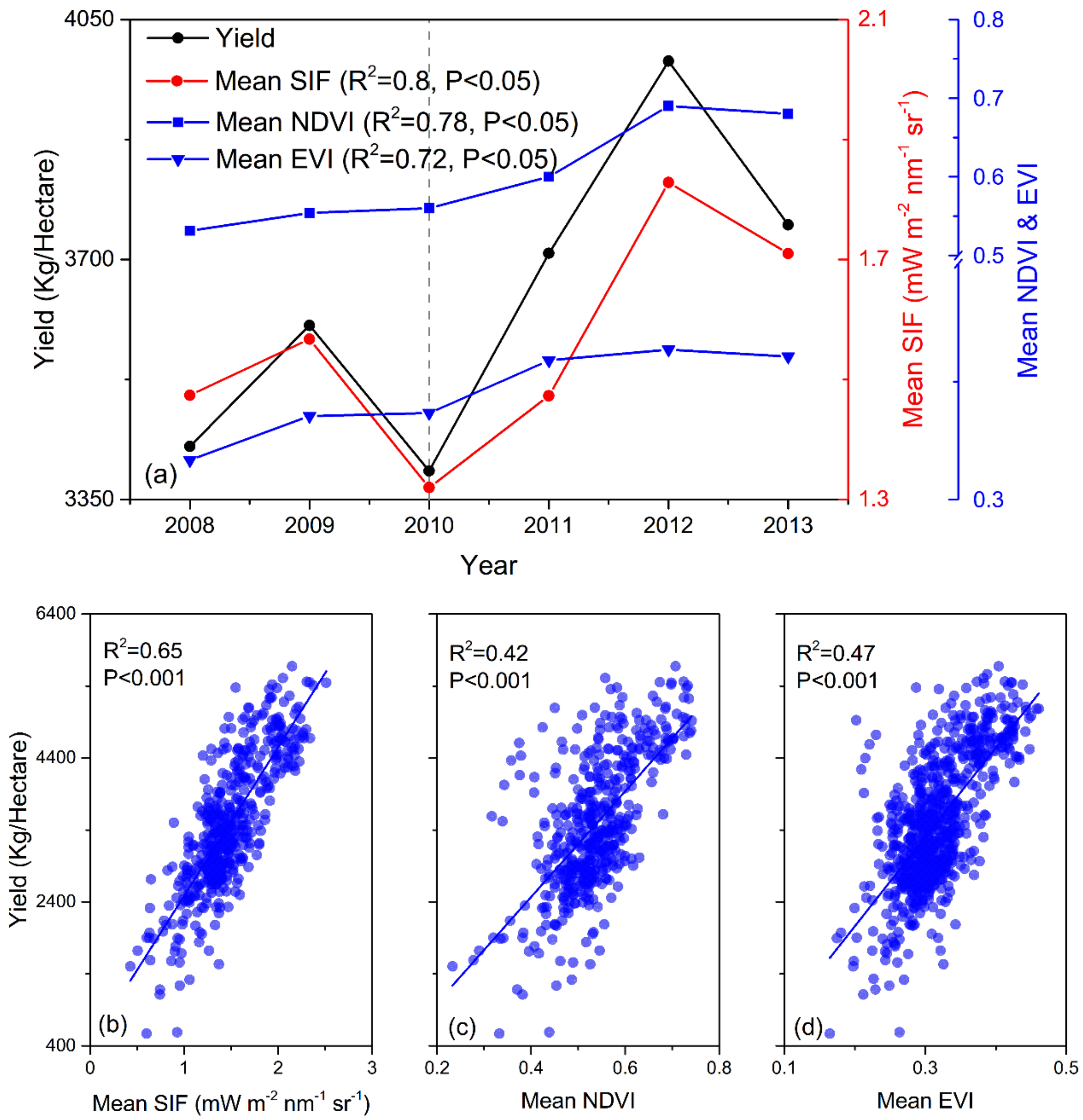


Figure 2. The relationship between yield and the mean SIF, NDVI and EVI during the wheat-growing season. (a) Interannual variations of yield, SIF, NDVI and EVI from 2008 to 2013 in the

IGP area, the values of $R^2$ and P indicate the linear fit between SIF/NDVI/EVI and yield. (b, c & d) Scatter plots of NPP against the mean SIF, NDVI and EVI during wheat growing season at the county scale, each dot represents the mean SIF/NDVI/EVI/Yield value during wheat growing season of one county and one year during 2008-2013.

*3.2 Spatiotemporal dynamics of the 2010 heat stress effects*

Heat stress is known to have a large impact on wheat growth and the final yield of the study region. The temperature on day of year (DOY) 65 of 2010 (which corresponds with the second half of February) shows a large increase (2.1±1.4℃ higher than the multiyear mean, Figure 3-a & b). The satellite observations of SIF show a quick response to this temperature increase with a reduction of approximately 4.5% (Figure 3-c & d). However, NDVI and EVI are not able to capture the heat stress effects until DOY 81, which is half a month later than the SIF response (Figure 3-e & f). Then, on DOY 97 (which corresponds with the first half of April), the temperature deviations from climatology are highest, resulting in an increase of 3.1±2.0℃ with respect to the multiyear mean. During this period, SIF declines approximately 37.9%, which is a much larger decrease than NDVI (-7.8%) and EVI (-11.9%). The results from the monthly variations of GOSAT SIF also demonstrate the similar pattern as GOME-2 SIF, confirming that the satellite observations of SIF are more sensitive to heat stress than VIs (Figure S2). Therefore, our results indicate that satellite SIF can capture the temporal dynamics of heat stress on winter wheat and show higher sensitivity in terms of temporal scale and the magnitude of the response than VIs.

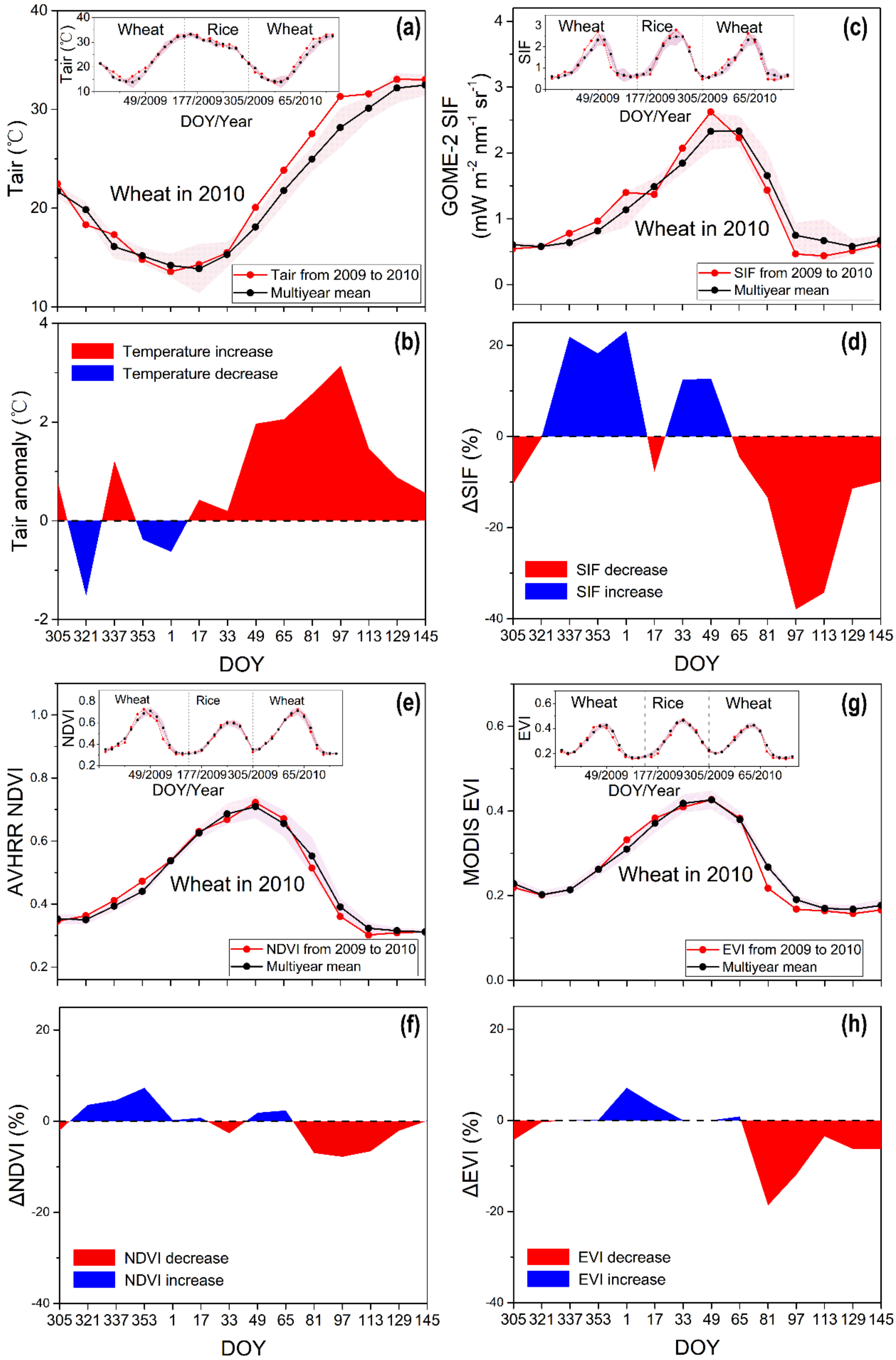


Figure 3. Seasonal variations from December 2009 to May 2010 of the 16-day mean and multiyear mean (a) air temperature (Tair) and (b) its anomaly, (c) GOME-2 SIF and (d) SIF change percent, (e) AVHRR NDVI and (f) NDVI change percent, (g) MODIS EVI and (h) EVI change percent over the

entire study area. The figures in the top-left corner of Figure a, c, e & g show the seasonal cycles of temperature, SIF and NDVI from 2009 to 2010.

The spatial and temporal distributions of temperature, SIF, NDVI and EVI provide additional insights into the dynamics of the wheat responses during the 2010 heat stress in the study area. The 2010 heat stress gradually evolves over space and expands from the northwest to the southeast. From February to April, the extreme warming moves from Punjab in the northwest to Haryana and Uttar Pradesh in the southeast, where there is widespread moderate heat stress (Figure 4 and 5). The positive temperature anomalies are the largest in April, especially in Punjab where the heat stress is extreme (3.5℃ higher than multiyear-mean value) (Figure 4-a and S3). As the temperatures increase, the soil moisture (SM) shows a slight decrease (Figure 4-c) with the largest reduction of only approximately -0.05 $m^3/m^3$ but with an uncertainty ~0.1 $m^3/m^3$ (Figure S4). This result confirms that water stress is not a limiting factor for wheat as the IGP is a well-irrigated area. On the other hand, the vapor pressure deficit (VPD) increases significantly, which is mostly driven by the higher temperatures and reduced relative humidity over the region (Figure 4-d).

With the development of the heat stress over the region, distinct responses to heat stress are found between SIF and NDVI/EVI over space and time. In March of 2010, approximately 88% of the region suffers from moderate stress (air temperature anomalies>1℃), and approximately 49% of the region area is affected by severe stress (>2℃) (Figure 4-a & b). Thus, 65% of the wheat in the study area is affected by moderate (<-0.5σ) losses as indicated by SIF, and 24% for severe losses (<-1σ). The moderate and severe loss percentages indicated by NDVI are approximately 37% and 14%, and the values for EVI are 12% and 7%, both of which underestimate the losses by nearly 50% compared to SIF (Figure 5-a & b). As the area influenced by heat stress expands, approximately 100% of the area suffers from moderate or severe heat stress, and 42% of the area suffers from extreme heat stress (>3℃) in April. As expected, SIF shows a much larger area with declines and more consistent declines with heat stress than NDVI and EVI. Approximately 76% and 36% of the area suffers from moderate and severe losses indicated by SIF, compared to the 43% and 11% indicated by NDVI. For extreme losses (<-1.5σ), the area percent revealed by SIF is 10%, while NDVI or EVI can not capture the losses at this heat stress level. MODIS EVI indicates the areas that suffer from moderate and severe losses are 56% and 17%, although these estimations are larger than those from NDVI, they are still much smaller than those estimated by SIF (Figure 5-b). The spatial distribution results of 2010 yield anomalies indicate that almost 100% area (except four counties) suffers the yield loss compared with the multiyear mean yield value during 2008-2013 (Figure 6), which is more consistent with the spatial distribution results of SIF. Overall, satellite observations of SIF capture the dynamics process of heat stress development in a timely manner, especially during March and April of 2010 (Figure 4 and 5).

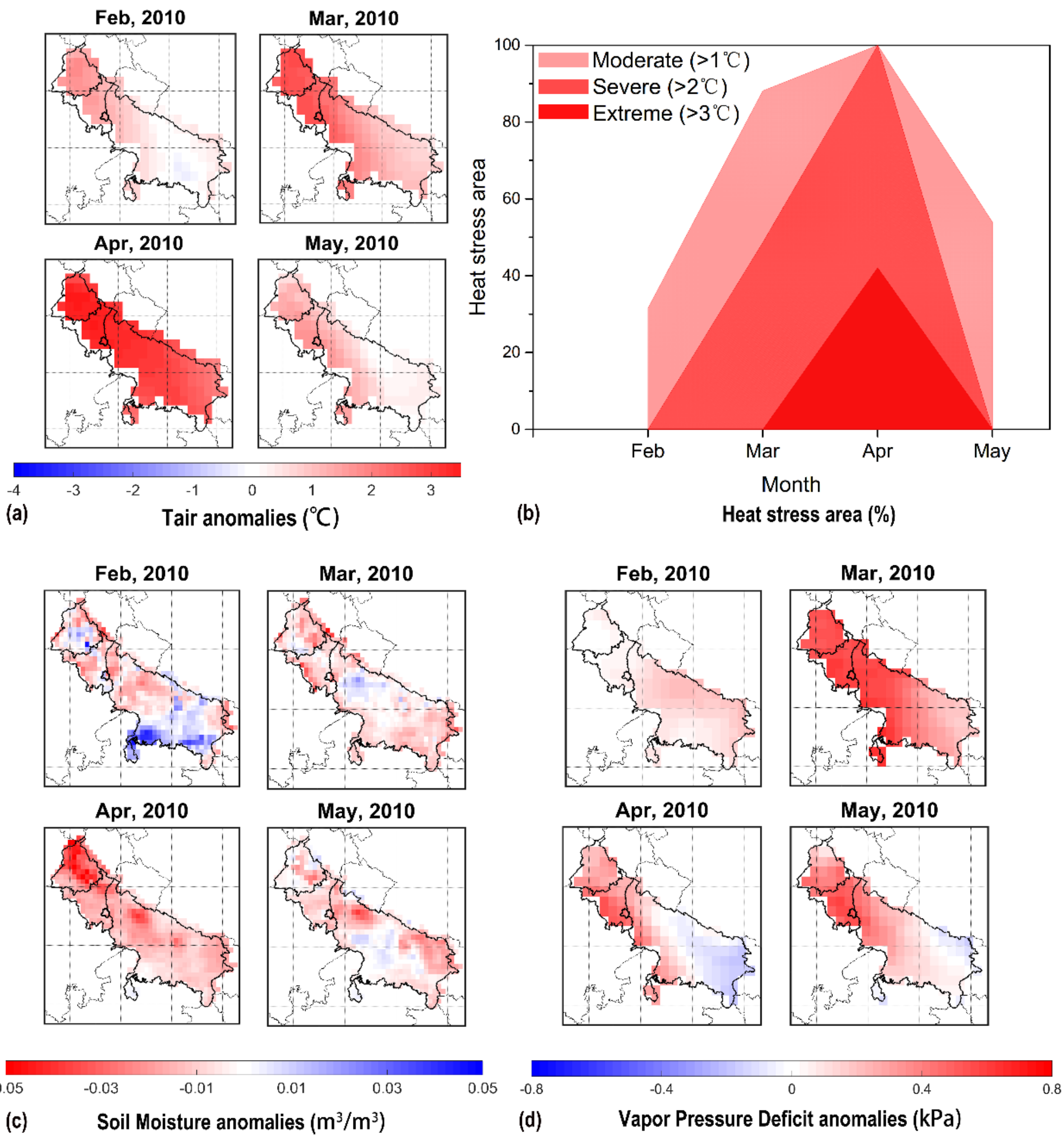


Figure 4. Spatial distribution of (a) temperature anomalies, (c) soil moisture anomalies and (d) vapor pressure deficit (VPD) anomalies from February to May of 2010 in the study area. (b) Monthly time series of the percentage of the area moderately (>1℃), severely (>2℃) and extremely (>3℃) influenced by heat stress.

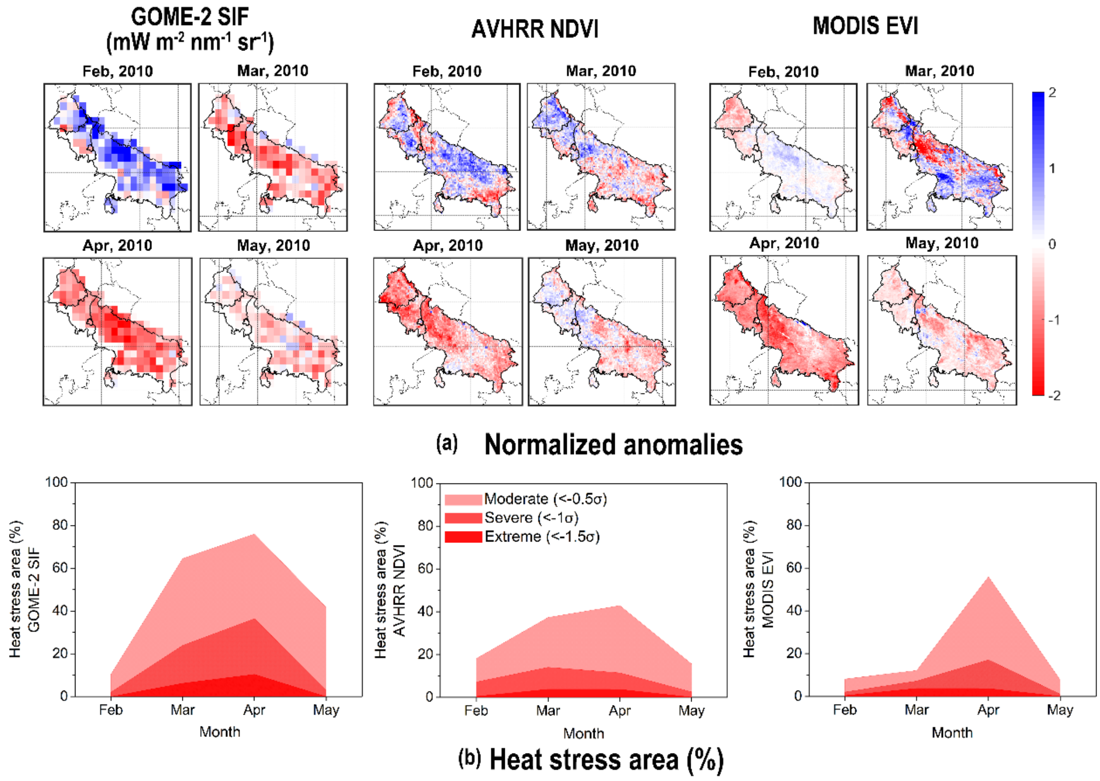


Figure 5. (a) Spatial distributions of normalized SIF, NDVI and EVI anomalies compared to the multiyear mean value during 2007-2014. (b) Monthly time series of the percentage of the wheat loss that was induced by heat stress, as indicated by SIF, NDVI and EVI under moderate (<-0.5σ), severe (<-1σ) and extreme (<-1.5σ) heat stress, σ indicates the standard deviation of the monthly SIF/NDVI/EVI during 2007-2014.

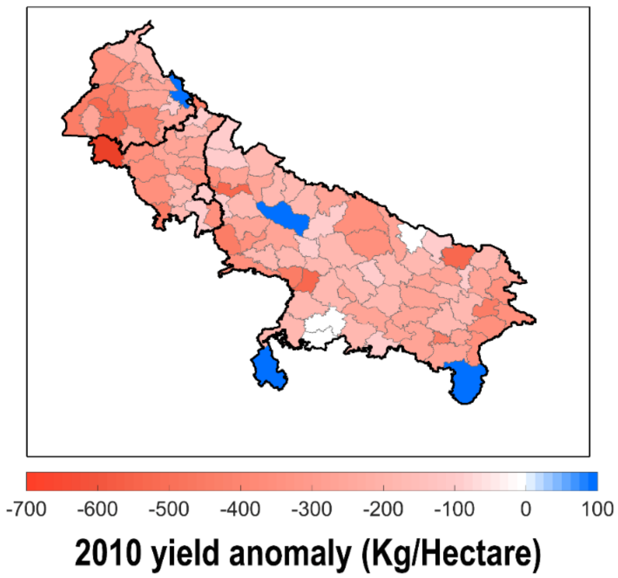


Figure 6. Spatial distributions of 2010 yield anomalies compared with the multiyear mean yield value from 2008-2013 at the county scale.

*3.3 Physiological response of wheat to the 2010 heat stress*

Since SIF is related to both APAR and fluorescence yield (as a physiological status), spaceborne retrievals of SIF may provide additional information on the response of wheat to heat stress. As shown in Figure 7, when the effects of seasonal variations in APAR are removed from the SIF (as indicated by $SIF_{yield}$) (equation (4)), the impacts of the 2010 heat stress on wheat become more distinct. In March, the fPAR shows a slight decrease, of approximately 2% from its multiyear mean value. At the same time, NDVI and EVI, which are mainly sensitive to fPAR, also show a slight negative change percent (-1.6% and -6% separately). The $SIF_{yield}$, which is sensitive to the fluorescence yield at the membrane scale and light use efficiency (LUE), shows negative anomalies (about -6% from its multiyear mean, Figure 7-b & c). The decline of the $SIF_{yield}$ along with the fPAR ultimately lead to the large and earlier decreases in March (approximately -11.2%). The spatial distributions also show that the $SIF_{yield}$ has a large reduction in March across the entire region (Figure 7-d). As indicated by the spatial distributions of NDVI and EVI in March of 2010, there are smaller changes compared with their own multiyear-mean results across the entire region (Figure 5-c).

In April, when the heat stress peaks, there is a decrease of only 4% in fPAR, the reductions of NDVI and EVI is approximately 8% and 7.8% separately, and $SIF_{yield}$ by 13%. The decreases in fPAR and $SIF_{yield}$ together lead to a significant decrease in SIF of 35%. The slower and smaller magnitude of the reductions in NDVI and fPAR suggest a slower effect of chlorophyll content and canopy structure in response to heat stress.

In contrast, the large and significantly negative anomalies in SIF along with $SIF_{yield}$ indicate that the anomalies of SIF are jointly driven by fPAR and LUE reductions. Our results thus suggest that both fPAR and fluorescence yield are influenced by heat stress, but with a larger contribution from physiological aspects ($SIF_{yield}$).

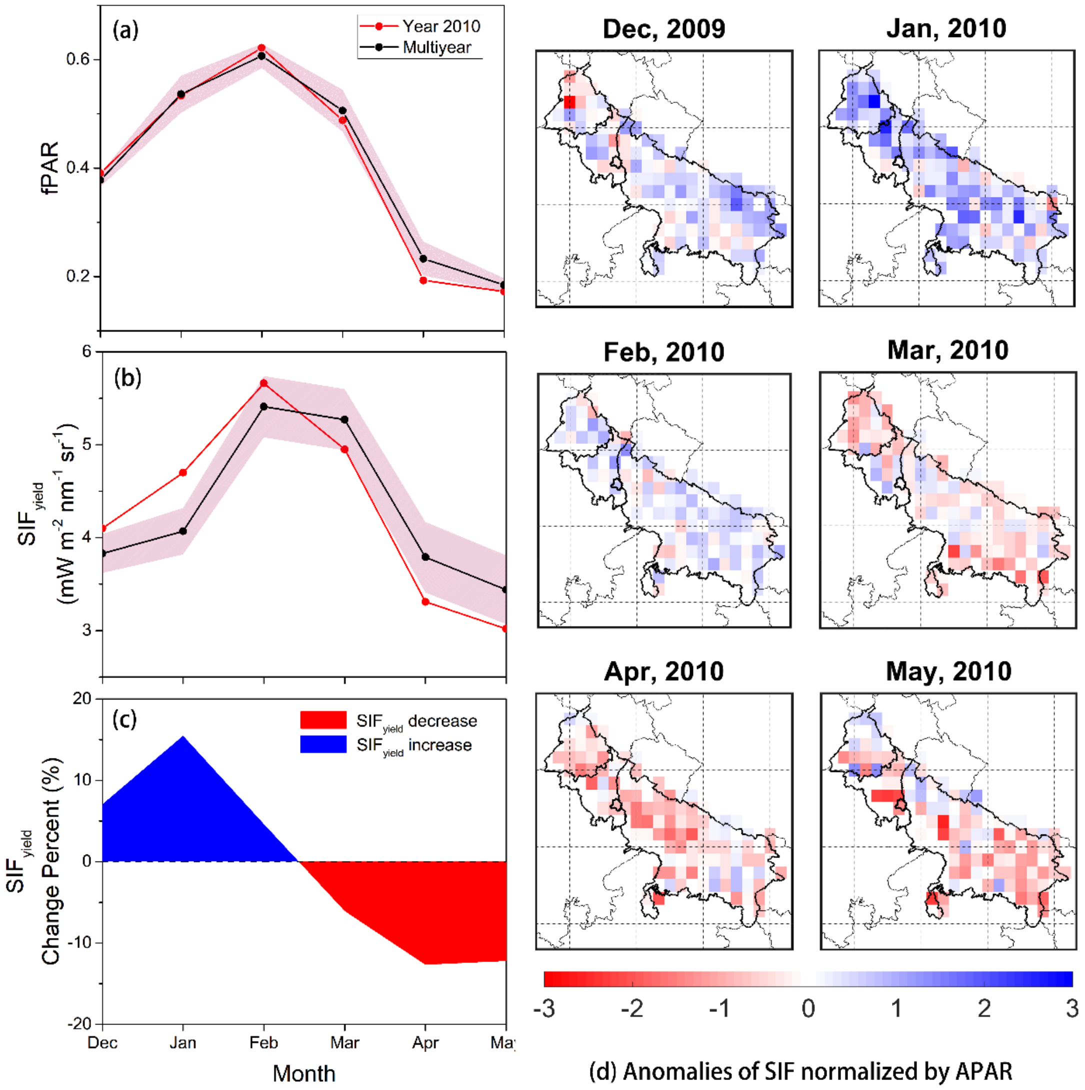


Figure 7. Temporal variations of (a) the fraction of absorbed photosynthetically active radiation (fPAR), (b) GOME-2 SIF normalized by absorbed photosynthetically active radiation ($SIF_{yield}$), (c) the $SIF_{yield}$ change percent, and (d) the spatial variations of the $SIF_{yield}$ anomalies from December 2009 to May 2010.

## 4. Discussion

With increasing global mean temperatures, crops are at risk of being exposed to heat stress that negatively affects crop yield (Lobell et al. 2012; Zhao et al. 2017; Asseng et al. 2011). It is therefore important to improve the monitoring and assessment of heat stress impacts on crop yields. In this study, we use the newly available spaceborne SIF measurements to monitor the heat stress on winter wheat in north-west India, which provides a new approach to understand the impacts of climate change on crop yields.

### *4.1 Potential of SIF for heat stress monitoring in wheat*

Spaceborne SIF observations capture the interannual variations of wheat yield better than NDVI and EVI at both the regional and county scales in the IGP (Figure 1). The advantage is especially more pronounced at the county scale. In 2010, corresponding to the large yield losses due to heat stress, both NDVI and EVI show an underestimation of the yield reduction. One possible reason for this underestimation may be due to the signal noise from background effects such as soil color, shadows or other non-green landscape components (Filella et al. 2004; Hilker et al. 2010; Bannari et al. 1995). Another possible reason for this underestimation is the insensitivity of the VIs to the actual photosynthetic activities of crops. Thus, many previous studies have focused on using greenness-based VI metrics along with other climatology data to quantify yield variations and may underestimate the yield loss effects (Prasad et al. 2006; Quarmby et al. 1993; Idso et al. 1977; Lobell et al. 2003; Xie et al. 2017). On the other hand, compared with VIs, chlorophyll fluorescence originals from the photosynthetic apparatus, so the background has a smaller impact on the fluorescence signal (Baker 2008). In this study, we show that using satellite SIF alone, which is more directly related to the photosynthetic functioning of crops, gives a better estimation of the final wheat yield than VIs. This study confirms an earlier study by Guan et.al. (2016), which showed that using spaceborne SIF-based GPP from GOME-2 can improve the crop yield estimations in the United States compared to standard VIs and other existing NPP products, and also demonstrated that SIF has a high sensitivity to environmental stresses (e.g., high temperature) through autotrophic and carbon-use-efficiency (Guan et al. 2016).

Within the study area, the 2010 heat stress period lasts for around two months from March to April, which corresponds to the wheat grain-filling and harvesting stages. The grain-filling period will determine the crop's individual grain size and has a great influence on the final yield (Guan et al. 2017; Lobell et al. 2012). High temperatures during this period can result in decreases in grain weight at maturity and has an adverse effect on wheat productivity (Wardlaw 1994). The linear fit results between yield and SIF/NDVI/EVI of March and April in our study are consistent with these previous studies. Especially during April, the SIF/NDVI/EVI have a significant positive relationship with wheat yield, and the April SIF can explain approximately 77% of the final yield (Figure S6 & S7).

Due to the sensitivity to canopy structure and pigment content (Garbulsky 2013), a large number of previous studies have focused on the estimations of plant pigment concentrations or vegetation productivity using greenness-based VIs (Gitelson et al.

1998; Blackburn 1999; Sims et al. 2002; Gamon et al. 2015; Beck et al. 2011). However, only a few studies monitored the rapid changes in plant photosynthetic activities induced by flash environmental stress. In contrast, as a good proxy of the actual photosynthetic activities in plants (Guanter et al. 2014; Sun et al. 2017), satellite SIF has been shown to nicely track the impacts of water stress or drought on various vegetation types (Lee et al. 2013; Sun et al. 2015; Yoshida et al. 2015; Guan et al. 2015). Extending upon these studies, we find that spaceborne SIF can be used to monitor heat stress in wheat crops in near real-time at large scales, and SIF can detect earlier and more pronounced responses to heat stress than NDVI and EVI. This result is consistent with previous studies, which showed that the vegetation indices appear to lag by half a month after the changes in temperature and precipitation (Wang et al. 2003). Since the GIMMS 3g AVHRR NDVI data are not fully atmospherically corrected, a Maximum Value Composites (MVC) technique is used to minimize the effects of changing illumination, viewing conditions, aerosols and cloud cover (Marçal et al. 1997). For the sake of consistency, we applied the same MVC technique to GOME-2 SIF data. The results from GOME-2 $SIF_{MVC}$ show no significant difference with the original SIF results (Figures S8 and S9): $SIF_{MVC}$ indicate earlier and more pronounced responses to heat stress than AVHRR NDVI, and the wheat growing season mean calculated from $SIF_{MVC}$ can also capture the 2010 yield loss due to heat stress. It should be noted that the MODIS EVI is derived from atmospherically-corrected reflectance, and then based on the product quality assurance metrics and constrained view angle approach to generate the 16-day composite data. Thus, the processing method of MODIS EVI is similar to the original GOME-2 SIF. Both the original SIF and $SIF_{MVC}$ indicate an earlier and more pronounced response to high temperatures than MODIS EVI.

### *4.2 Improved understanding on the responses of crops to heat stress*

From the temporal and spatial results of fPAR and $SIF_{yield}$, we have gained a better understanding of the mechanisms of the 2010 heat stress, and have also been able to attribute the SIF responses under heat stress conditions to a certain extent. In the early stage of this heat stress, the VPD increases, which results in stomatal closure and the decline of both $CO_2$ uptake and the photosynthetic functioning of wheat in the study area (Dai et al. 1992) (Figure 4-d & S4). Experimental studies on the ground documented that when plants were exposed to high temperatures even for a short time, the photosynthetic rates showed remarkable declines, especially in terms of the PSII activity (Al-Khatib et al. 1990). At the site scale, vegetation fluorescence was shown to be effective in detecting the decline in the plants photosynthetic capacity (Sobrino 2002; Louis et al. 2005). In this study, we extend this research to a large scale, and investigate the relative contribution of fPAR and $SIF_{yield}$ to the SIF reduction under extremely high temperature conditions. We find that there is a small change of fPAR along with NDVI, but the real change in $SIF_{yield}$ may suggest that most wheat crops in the study area remain green while their photosynthetic capacities decrease during the early stage of this stress. SIF and $SIF_{yield}$ show decreases earlier than NDVI and EVI. This suggests that SIF can be extended from the site scale to a larger scale to monitor the changes in the actual photosynthetic activities of crops. Similar results were also found in the 2010 Russian drought revealed by GOME-2 SIF and MODIS NDVI, in which Yoshida et al. (2015) found that SIF normalized by PAR decreased rapidly as compared with the NDVI during the senescence stage across various vegetation types. It should be noted that wheat canopy structure may also change under high stress levels, and hence the constant assumption of $\Omega_c$ is not reliable. In this case, the reduction of $SIF_{yield}$ may also partly attributed to the changes of canopy structure. Thus, SIF escaping probability due to reabsorption of SIF and canopy structure should also be considered in future studies when interpreting $SIF_{yield}$ (Joiner et al. 2014).

The larger negative anomalies of SIF compared to NDVI and fPAR during the 2010 heat stress period suggest that there are decreases in both the photosynthesis capacities and greenness of wheat crops, and the decline of the latter can be reflected by both SIF and VIs. The combined decreases of wheat photosynthesis and greenness lead to the more pronounced response of SIF reduction to this heat stress and ultimately the reductions of wheat crop yields in this region. One specific reason for this reduction in yield may be the earlier senescence of physiology that is caused by the extreme high temperatures during the grain-filling stage, which lead to a shortened of the wheat growing season (Figure S1). This ultimately results in the reduction of the final kernel weight, a key determinant of the yield (Dias et al. 2009). This finding is consistent with previous studies. Lobell et al. 2012 found that extremely high temperatures had a strong effect on the wheat growing season length (GSL) in IGP area and could result in a shorter GSL (Lobell et al. 2012). Joiner et al. 2014 compared GOME-2 SIF and tower-based GPP, and the results indicated that satellite SIF data achieved similar performance at detecting the shortened GSL at an agricultural site in Nebraska as the GPP measures on the ground (Joiner et al. 2014). The shortened GSL of wheat due to high temperatures indicates that some suitable management strategies, such as altering sowing dates or harvesting dates to avoid the high temperatures, can reduce the effect of heat stress on crops (Gourdji et al. 2013).

*4.3 Implications for the monitoring and assessment of heat stress impacts on crops*

Sustainably producing more food is a global challenge. This task is daunting as less land is available for agricultural exploitation and the temperatures and frequencies of droughts are increasing (IPCC 2014; Foley et al. 2011; Tilman et al. 2011). Agricultural adaptation requires accurate and timely crop monitoring in response to warming, especially with an increase in global temperature and frequency of extremely high-temperature events (Gourdji et al. 2013). In this paper, we demonstrate that satellite SIF observations have much better ability to detect and track the 2010 heat stress than the widely used greenness-based VIs over the intensely managed wheat regions in the IGP, the food bowl of India. This finding highlights that the new spaceborne measurements of SIF can be used as early warning tools for stress detection in large agricultural regions before harvest, particularly during the grain-filling stage when photosynthesis is sensitive to climate factors. However, considering that the current available instruments were not primarily designed for SIF retrievals and the associated uncertainties of the retrievals, further in situ field measurements of SIF and controlled experiments are needed to strength our understanding of how biochemical mechanisms and environmental factors control SIF (Miao et al. 2018; Schlau-Cohen et al. 2015).

Our results could have a range of implications for both research and policy. First, accurate and timely monitoring of heat stress at large scales could better enable the evaluations of their impacts on wheat yields. As there are lags in the response to heat stress from the greenness-based VIs (Wang et al. 2003) and uncertainties in crop models (Asseng et al. 2015), SIF can be an independent tool to monitor and assess the impacts of warming on wheat production in a timely manner. In particular, more accurate evaluations of the impacts of heat stress could be conducted by improving the spatial and temporal resolution of the satellite SIF in the near future. Second, the ability to detect wheat senescence to heat stress over a large scale and in a timely manner could help policy-makers or farmers target appropriate mitigation strategies during the critical grain filling stage. Field experimental studies have shown that irrigation managements that match with the grain filling stage can offset the heat stress impacts on wheat in Haryana, India (Gupta et al. 2010).

The earlier detection from SIF could provide insights for adaption for agricultural practices. As indicated by SIF, the wheat with earlier sowing dates in Punjab in the northwest of the study area suffered from fewer losses, but the wheat in the central part of the study area experienced more losses, which suggest that climate smart agricultural (CSA) practices such as zero-tillage can also compensate for the impacts of heat stress on wheat to some extent (Campbell et al. 2014). However, although the SIF results indicate a shortening of wheat growing season length due to extreme high temperatures, the adoption of certain managements practices such as earlier transplanting date can partly mitigate heat impacts on wheat growth, to what extent these management practices can mitigate climate impacts remain uncertain. Crop models are generally used to separate climate change impacts from management practices on the length of the rice growing period (Wang et al. 2017). Thus, incorporating satellite SIF data into crop models may provide better constraints to phenology simulations, and further improve the modelling of crops' response to climate change.

In the IGP during wheat growing period, extreme high temperatures usually occur in March and April. Thus, advancing the planting time can make wheat key growing phase escape the extremely high temperatures period and avoid yield penalty due to heat stress. However, when the temperature increases in the cropping regions exceed a certain threshold (3.5°C higher than the multiyear-mean value in this study), this method will be less effective. Thus, more adaptation strategies need to be implemented, such as breeding new wheat varieties that have a higher tolerance to warming temperatures. Finally, the spatial and temporal patterns of the effects of heat stress that are captured in the satellite SIF data, especially the physiological response to warming, provide a useful new data set that can be used as a benchmark for the widely used crop models (Asseng et al. 2013). In particular, the use of spaceborne SIF measurements could complement the existing VIs and provide more directly measurable signals of crop photosynthetic activities. These measurements would help address the broader scale questions that have been increasingly addressed by crop simulation models to evaluate the impacts of climate change (Lobell et al. 2012; Asseng et al. 2015).

For future applications, improved SIF datasets would be needed at better spatial and temporal resolution, even at the subdaily scale. Higher spatial and temporal resolution SIF products are anticipated from several new satellite instruments such as TROPOMI with a high spatial resolution of $7\times3.5m^2$ at nadir (successfully launched on 13 October 2017 on board the Sentinel 5 (Guanter et al. 2015)), the NASA TEMPO instrument (to be launched in 2019, (Chance et al. 2013)), the ESA Sentinel-4/UVN instrument (to be launched in 2019, (Stark et al. 2012)), and the GeoCARB instrument (Rayner et al. 2014). The current SIF data employed in this study are measured by GOME-2, which has a morning overpass time, future satellite missions such as the launched TROPOMI (the overpass time is 13:30 at local time) will improve the monitoring of heat stress in plants. Although more satellite instruments capable of generating SIF products at higher spatial and temporal resolution will be launched in the near future, SIF product availability has a large delay after the satellite data acquisition. Thus, it will be essential to further improve processing algorithms and data distribution so that the SIF product latency to the user community can be reduced.

In summary, this work shows that spaceborne SIF can be an effective tool to monitor heat stress in wheat crops across the Haryana-Uttar belt in India. The high correlations between SIF and the yield at both large and small scales demonstrate that spaceborne SIF can be a good proxy for crops yields. In addition, spaceborne SIF and $SIF_{yield}$ show earlier and more pronounced responses to extreme high temperatures than the greenness VIs, which indicate that satellite SIF observations are sensitive to both the structural and physiological variations of plants and can be used to monitor the heat stress on crops at near real-time over a large scale. The various wheat losses induced by heat stress in Punjab and the central part of the study region suggest that the earlier sowing dates resulting from the zero-tillage of the CSA in India can offset the influence of heat stress to some extent. However, with the continuing increase in global warming and extreme events, better strategies need to be implemented to further reduce the temperature-induced yield loss.

**Acknowledgments**

This research by L.S. and Y.Z. is financially supported by the National Key R&D Program of China (2016YFA0600202), Jiangsu Provincial Natural Science Fund for Distinguished Young Scholars of China (BK20170018), the International Cooperation and Exchange Programs of National Science Foundation of China (Sino-German, 41761134082), and General Program of National Science Foundation of China (41671421). This study is also partially supported by the Emmy Noether Programme (GlobFluo project) of the German Research Foundation (Grant NO.: GU 1276/1-1). MODIS MOD13 EVI/NDVI data were obtained from the MODIS LP DAAC archive, and GIMMS NDVI from https://ecocast.arc.nasa.gov/data/pub/gimms/3g.v1/. Kaiyu Guan acknowledges the support from the Institute for Sustainability, Energy, and

Environment (iSEE) of University of Illinois at Urbana Champaign.

**Conflict of interest**

The authors declare that they have no conflicts of interest.

## Reference


Al-Khatib, K. & G. M. Paulsen (1990) Photosynthesis and Productivity during High-Temperature Stress of Wheat Genotypes from Major World Regions. *Crop Science,* 30, 1127-1132.

Asseng, S.,F. Ewert,P. Martre,R. P. Rötter,D. Lobell,D. Cammarano,B. Kimball,M. Ottman,G. Wall & J. W. White (2015) Rising temperatures reduce global wheat production. *Nature Climate Change,* 5, 143.

Asseng, S.,F. Ewert,C. Rosenzweig,J. Jones,J. Hatfield,A. Ruane,K. J. Boote,P. J. Thorburn,R. P. Rötter & D. Cammarano (2013) Uncertainty in simulating wheat yields under climate change. *Nature Climate Change,* 3, 827-832.

Asseng, S.,I. A. N. Foster & N. C. Turner (2011) The impact of temperature variability on wheat yields. *Global Change Biology,* 17, 997-1012.

Baker, N. R. (2008) Chlorophyll fluorescence: a probe of photosynthesis in vivo. *Annu Rev Plant Biol,* 59, 89-113.

Bannari, A.,D. Morin,F. Bonn & A. Huete (1995) A review of vegetation indices. *Remote sensing reviews,* 13, 95-120.

Barton, C. V. M. & P. North (2001) Remote sensing of canopy light use efficiency using the photochemical reflectance index: Model and sensitivity analysis. *Remote Sensing of Environment,* 78, 264-273.

Beck, P. S. & S. J. Goetz (2011) Satellite observations of high northern latitude vegetation productivity changes between 1982 and 2008: ecological variability and regional differences. *Environmental Research Letters,* 6, 045501.

Blackburn, G. A. (1999) Relationships between spectral reflectance and pigment concentrations in stacks of deciduous broadleaves. *Remote Sensing of Environment,* 70, 224-237.

Bryant-Erdmann, S. 2017. Wheat: Less Acres in 2017-18, But Still Third Largest Crop Ever. In *AgFax*. USW Market Analyst.

Campbell, B. M.,P. Thornton,R. Zougmoré,P. van Asten & L. Lipper (2014) Sustainable intensification: What is its role in climate smart agriculture? *Current Opinion in Environmental Sustainability,* 8, 39-43.

Challinor, A. J.,T. R. Wheeler,J. M. Slingo,P. Q. Craufurd & D. I. F. Grimes (2005) Simulation of Crop Yields Using ERA-40: Limits to Skill and Nonstationarity in Weather–Yield Relationships. *Journal of Applied Meteorology,* 44**,** 516-531.

Chance, K. V.,X. Liu,R. M. Suleiman,D. E. Flittner,J. Al-Saadi & S. J. Janz. 2013. Tropospheric emissions: monitoring of pollution (TEMPO). SPIE-International Society for Optical Engineering.

Chappelle, E. W.,F. M. Wood,J. E. McMurtrey & W. W. Newcomb (1984) Laser-induced fluorescence of green plants. 1: A technique for the remote detection of plant stress and species differentiation. *Applied Optics,* 23**,** 134-138.

Chappelle, E. W.,F. M. Wood,W. W. Newcomb & J. E. McMurtrey (1985) Laser-induced fluorescence of green plants. 3: LIF spectral signatures of five major plant types. *Applied optics,* 24**,** 74-80.

Chauhan, B. S.,G. Mahajan,V. Sardana,J. Timsina & M. L. Jat (2012) Productivity and sustainability of the rice-wheat cropping system in the Indo-Gangetic Plains of the Indian subcontinent: problems, opportunities, and strategies. *Advances in Agronomy,* 117**,** 315-369.

Dai, Z.,G. E. Edwards & M. S. Ku (1992) Control of photosynthesis and stomatal conductance in Ricinus communis L.(castor bean) by leaf to air vapor pressure deficit. *Plant Physiology,* 99**,** 1426-1434.

Dias, A. S. & F. C. Lidon (2009) Evaluation of Grain Filling Rate and Duration in Bread and Durum Wheat, under Heat Stress after Anthesis. *Journal of Agronomy and Crop Science,* 195**,** 137-147.

Dobrowski, S.,J. Pushnik,P. Zarco-Tejada & S. Ustin (2005) Simple reflectance indices track heat and water stress-induced changes in steady-state chlorophyll fluorescence at the canopy scale. *Remote Sensing of Environment,* 97**,** 403-414.

Duncan, J.,J. Dash & P. M. Atkinson (2015) Elucidating the impact of temperature variability and extremes on cereal croplands through remote sensing. *Global change biology,* 21**,** 1541-1551.

Erenstein, O. (2009) Comparing water management in rice–wheat production systems in Haryana, India and Punjab, Pakistan. *Agricultural Water Management,* 96, 1799-1806.

Field, C. B. 2012. *Managing the risks of extreme events and disasters to advance climate change adaptation: special report of the intergovernmental panel on climate change*. Cambridge University Press.

Filella, I.,J. Penuelas,L. Llorens & M. Estiarte (2004) Reflectance assessment of seasonal and annual changes in biomass and CO 2 uptake of a Mediterranean shrubland submitted to experimental warming and drought. *Remote Sensing of Environment,* 90, 308-318.

Foley, J. A.,N. Ramankutty,K. A. Brauman,E. S. Cassidy,J. S. Gerber,M. Johnston,N. D. Mueller,C. O'Connell,D. K. Ray & P. C. West (2011) Solutions for a cultivated planet. *Nature,* 478, 337.

Frankenberg, C.,J. B. Fisher,J. Worden,G. Badgley,S. S. Saatchi,J.-E. Lee,G. C. Toon,A. Butz,M. Jung,A. Kuze & T. Yokota (2011) New global observations of the terrestrial carbon cycle from GOSAT: Patterns of plant fluorescence with gross primary productivity. *Geophysical Research Letters,* 38, n/a-n/a.

Frankenberg, C.,C. O'Dell,J. Berry,L. Guanter,J. Joiner,P. Köhler,R. Pollock & T. E. Taylor (2014) Prospects for chlorophyll fluorescence remote sensing from the Orbiting Carbon Observatory-2. *Remote Sensing of Environment,* 147, 1-12.

Friedl, M. A.,D. Sulla-Menashe,B. Tan,A. Schneider,N. Ramankutty,A. Sibley & X. Huang (2010) MODIS Collection 5 global land cover: Algorithm refinements and characterization of new datasets. *Remote sensing of Environment,* 114, 168-182.

Gamon, J.,C. Field,W. Bilger,O. Björkman,A. Fredeen & J. Peñuelas (1990) Remote sensing of the xanthophyll cycle and chlorophyll fluorescence in sunflower leaves and canopies. *Oecologia,* 85, 1-7.

Gamon, J.,O. Kovalchuck,C. Wong,A. Harris & S. Garrity (2015) Monitoring seasonal and diurnal changes in photosynthetic pigments with automated PRI and NDVI sensors. *Biogeosciences,* 12, 4149-4159.

Gamon, J.,J. Penuelas & C. Field (1992) A narrow-waveband spectral index that tracks diurnal changes in photosynthetic efficiency. *Remote Sensing of environment,* 41, 35-44.

Gamon, J.,L. Serrano & J. Surfus (1997) The photochemical reflectance index: an optical indicator of photosynthetic radiation use efficiency across species, functional types, and nutrient levels. *Oecologia,* 112**,** 492-501.

Garbulsky, M. F. 2013. *Recent Advances in the Estimation of Photosynthetic Stress for Terrestrial Ecosystem Services Related to Carbon Uptake*. Argentina: University of Buenos Aires.

Gitelson, A. A. & M. N. Merzlyak (1998) Remote sensing of chlorophyll concentration in higher plant leaves. *Advances in Space Research,* 22**,** 689-692.

Gourdji, S. M.,A. M. Sibley & D. B. Lobell (2013) Global crop exposure to critical high temperatures in the reproductive period: historical trends and future projections. *Environmental Research Letters,* 8**,** 024041.

Guan, K.,J. A. Berry,Y. Zhang,J. Joiner,L. Guanter,G. Badgley & D. B. Lobell (2016) Improving the monitoring of crop productivity using spaceborne solar‐induced fluorescence. *Global change biology,* 22**,** 716-726.

Guan, K.,M. Pan,H. Li,A. Wolf,J. Wu,D. Medvigy,K. K. Caylor,J. Sheffield,E. F. Wood & Y. Malhi (2015) Photosynthetic seasonality of global tropical forests constrained by hydroclimate. *Nature Geoscience,* 8**,** 284.

Guan, K.,J. Wu,J. S. Kimball,M. C. Anderson,S. Frolking,B. Li,C. R. Hain & D. B. Lobell (2017) The shared and unique values of optical, fluorescence, thermal and microwave satellite data for estimating large-scale crop yields. *Remote Sensing of Environment,* 199**,** 333-349.

Guanter, L.,I. Aben,P. Tol,J. Krijger,A. Hollstein,P. Köhler,A. Damm,J. Joiner,C. Frankenberg & J. Landgraf (2015) Potential of the TROPOspheric Monitoring Instrument (TROPOMI) onboard the Sentinel-5 Precursor for the monitoring of terrestrial chlorophyll fluorescence. *Atmospheric Measurement Techniques,* 8**,** 1337-1352.

Guanter, L.,C. Frankenberg,A. Dudhia,P. E. Lewis,J. Gómez-Dans,A. Kuze,H. Suto & R. G. Grainger (2012) Retrieval and global assessment of terrestrial chlorophyll fluorescence from GOSAT space measurements. *Remote Sensing of Environment,* 121**,** 236-251.

Guanter, L.,Y. Zhang,M. Jung,J. Joiner,M. Voigt,J. A. Berry,C. Frankenberg,A. R. Huete,P. Zarco-Tejada,J.-E. Lee,M. S. Moran,G. Ponce-Campos,C. Beer,G. Camps-Valls,N. Buchmann,D.

Gianelle,K. Klumpp,A. Cescatti,J. M. Baker & T. J. Griffis (2014) Global and time-resolved monitoring of crop photosynthesis with chlorophyll fluorescence. *Proceedings of the National Academy of Sciences,* 111**,** E1327-E1333.

Gupta, R.,R. Gopal,M. Jat,R. K. Jat,H. Sidhu,P. Minhas & R. Malik. 2010. Wheat productivity in indo-gangetic plains of India during 2010: Terminal heat effects and mitigation strategies.

Gupta, R. & A. Seth (2007) A review of resource conserving technologies for sustainable management of the rice–wheat cropping systems of the Indo-Gangetic plains (IGP). *Crop protection,* 26**,** 436-447.

Hennessy, K.,R. Fawcett,D. Kirono,F. Mpelasoka,D. Jones,J. Bathols,P. Whetton,M. Stafford Smith,M. Howden & C. Mitchell (2008) An assessment of the impact of climate change on the nature and frequency of exceptional climatic events. *Australian Government Bureau of Meteorology: Melbourne*.

Hilker, T.,F. G. Hall,N. C. Coops,A. Lyapustin,Y. Wang,Z. Nesic,N. Grant,T. A. Black,M. A. Wulder & N. Kljun (2010) Remote sensing of photosynthetic light-use efficiency across two forested biomes: Spatial scaling. *Remote Sensing of Environment,* 114**,** 2863-2874.

Idso, S. B.,R. D. Jackson & R. J. Reginato (1977) Remote-sensing of crop yields. *Science,* 196**,** 19-25.

IPCC. 2014. *IPCC, 2014: Climate Change 2014: Synthesis Report. Contribution of Working Groups I, II and III to the Fifth Assessment Report of the Intergovernmental Panel on Climate Change*. IPCC.

Joiner, J.,L. Guanter,R. Lindstrot,M. Voigt,A. P. Vasilkov,E. M. Middleton,K. F. Huemmrich,Y. Yoshida & C. Frankenberg (2013) Global monitoring of terrestrial chlorophyll fluorescence from moderate-spectral-resolution near-infrared satellite measurements: methodology, simulations, and application to GOME-2. *Atmos. Meas. Tech.,* 6**,** 2803-2823.

Joiner, J.,Y. Yoshida,A. Vasilkov,E. Middleton,P. Campbell & A. Kuze (2012) Filling-in of near-infrared solar lines by terrestrial fluorescence and other geophysical effects: Simulations and space-based observations from SCIAMACHY and GOSAT. *Atmospheric Measurement Techniques,* 5**,** 809-829.

Joiner, J.,Y. Yoshida,A. Vasilkov,K. Schaefer,M. Jung,L. Guanter,Y. Zhang,S. Garrity,E. Middleton &

K. Huemmrich (2014) The seasonal cycle of satellite chlorophyll fluorescence observations and its relationship to vegetation phenology and ecosystem atmosphere carbon exchange. *Remote Sensing of Environment,* 152**,** 375-391.

Koehler, A.-K.,A. J. Challinor,E. Hawkins & S. Asseng (2013) Influences of increasing temperature on Indian wheat: quantifying limits to predictability. *Environmental Research Letters,* 8**,** 034016.

Köhler, P.,L. Guanter & C. Frankenberg (2015) Simplified physically based retrieval of sun-induced chlorophyll fluorescence from GOSAT data. *IEEE Geoscience and Remote Sensing Letters,* 12**,** 1446-1450.

Köhler, P.,L. Guanter & J. Joiner (2015) A linear method for the retrieval of sun-induced chlorophyll fluorescence from GOME-2 and SCIAMACHY data. *Atmos. Meas. Tech.,* 8**,** 2589-2608.

Labus, M.,G. Nielsen,R. Lawrence,R. Engel & D. Long (2002) Wheat yield estimates using multi-temporal NDVI satellite imagery. *International Journal of Remote Sensing,* 23**,** 4169-4180.

Lee, J.-E.,C. Frankenberg,C. van der Tol,J. A. Berry,L. Guanter,C. K. Boyce,J. B. Fisher,E. Morrow,J. R. Worden & S. Asefi (2013) Forest productivity and water stress in Amazonia: observations from GOSAT chlorophyll fluorescence. *Proceedings of the Royal Society of London B: Biological Sciences,* 280**,** 20130171.

Lobell, D. B.,G. P. Asner,J. I. Ortiz-Monasterio & T. L. Benning (2003) Remote sensing of regional crop production in the Yaqui Valley, Mexico: estimates and uncertainties. *Agriculture, Ecosystems & Environment,* 94**,** 205-220.

Lobell, D. B.,A. Sibley & J. Ivan Ortiz-Monasterio (2012) Extreme heat effects on wheat senescence in India. *Nature Clim. Change,* 2**,** 186-189.

Louis, J.,A. Ounis,J.-M. Ducruet,S. Evain,T. Laurila,T. Thum,M. Aurela,G. Wingsle,L. Alonso & R. Pedros (2005) Remote sensing of sunlight-induced chlorophyll fluorescence and reflectance of Scots pine in the boreal forest during spring recovery. *Remote sensing of environment,* 96**,** 37-48.

Magney, T. S.,L. A. Vierling,J. U. Eitel,D. R. Huggins & S. R. Garrity (2016) Response of high frequency Photochemical Reflectance Index (PRI) measurements to environmental conditions in wheat. *Remote Sensing of Environment,* 173, 84-97.

Marçal, A. & G. Wright (1997) The use of'overlapping'NOAA-AVHRR NDVI maximum value composites for Scotland and initial comparisons with the land cover census on a Scottish Regional and District basis. *International Journal of Remote Sensing,* 18, 491-503.

Miao, G.,K. Guan,X. Yang,C. J. Bernacchi,J. A. Berry,E. H. DeLucia,J. Wu,C. E. Moore,K. Meacham & Y. Cai (2018) Sun-Induced Chlorophyll Fluorescence, Photosynthesis, and Light Use Efficiency of a Soybean Field from Seasonally Continuous Measurements. *Journal of Geophysical Research: Biogeosciences,* 123, 610-623.

Moya, I.,L. Camenen,S. Evain,Y. Goulas,Z. Cerovic,G. Latouche,J. Flexas & A. Ounis (2004) A new instrument for passive remote sensing: 1. Measurements of sunlight-induced chlorophyll fluorescence. *Remote Sensing of Environment,* 91, 186-197.

Myneni, R. B.,S. Hoffman,Y. Knyazikhin,J. Privette,J. Glassy,Y. Tian,Y. Wang,X. Song,Y. Zhang & G. Smith (2002) Global products of vegetation leaf area and fraction absorbed PAR from year one of MODIS data. *Remote sensing of environment,* 83, 214-231.

Pathak, H.,J. Ladha,P. Aggarwal,S. Peng,S. Das,Y. Singh,B. Singh,S. Kamra,B. Mishra & A. Sastri (2003) Trends of climatic potential and on-farm yields of rice and wheat in the Indo-Gangetic Plains. *Field Crops Research,* 80, 223-234.

Pinzon, J. E. & C. J. Tucker (2014) A non-stationary 1981–2012 AVHRR NDVI3g time series. *Remote Sensing,* 6, 6929-6960.

Porcar-Castell, A.,E. Tyystjärvi,J. Atherton,C. van der Tol,J. Flexas,E. E. Pfündel,J. Moreno,C. Frankenberg & J. A. Berry (2014) Linking chlorophyll a fluorescence to photosynthesis for remote sensing applications: mechanisms and challenges. *Journal of experimental botany,* 65, 4065-4095.

Prasad, A. K.,L. Chai,R. P. Singh & M. Kafatos (2006) Crop yield estimation model for Iowa using remote sensing and surface parameters. *International Journal of Applied Earth Observation and Geoinformation,* 8, 26-33.

Quarmby, N.,M. Milnes,T. Hindle & N. Silleos (1993) The use of multi-temporal NDVI measurements from AVHRR data for crop yield estimation and prediction. *International Journal of*

*Remote Sensing,* 14, 199-210.

Rayner, P. J.,S. Utembe & S. Crowell (2014) Constraining regional greenhouse gas emissions using geostationary concentration measurements: a theoretical study. *Atmospheric Measurement Techniques,* 7, 3285-3293.

Rohini, P.,M. Rajeevan & A. Srivastava (2016) On the variability and increasing trends of heat waves over India. *Scientific reports,* 6, 26153.

Schlau-Cohen, G. S. & J. Berry (2015) Photosynthetic fluorescence, from molecule to planet. *Physics Today,* 68.

Schöffl, F.,R. Prandl & A. Reindl (1999) Molecular responses to heat stress. *Molecular responses to cold, drought, heat and salt stress in higher plants*, 81-98.

Sims, D. A. & J. A. Gamon (2002) Relationships between leaf pigment content and spectral reflectance across a wide range of species, leaf structures and developmental stages. *Remote sensing of environment,* 81, 337-354.

Sobrino, J. A. 2002. *Recent advances in quantitative remote sensing*. Universitat de València.

Solano, R.,K. Didan,A. Jacobson & A. Huete (2010) MODIS vegetation index user's guide (MOD13 series). *Vegetation Index and Phenology Lab, The University of Arizona*, 1-38.

Stark, H. R.,H. L. Möller,G. B. Courrèges-Lacoste,R. Koopman,S. Mezzasoma & B. Veihelmann. 2012. The sentinel-4 mission, its components and implementation. The Netherlands: ESA ESTEC.

Sun, Y.,C. Frankenberg,J. D. Wood,D. S. Schimel,M. Jung,L. Guanter,D. T. Drewry,M. Verma,A. Porcar-Castell,T. J. Griffis,L. Gu,T. S. Magney,P. Köhler,B. Evans & K. Yuen (2017) OCO-2 advances photosynthesis observation from space via solar-induced chlorophyll fluorescence. *Science,* 358.

Sun, Y.,R. Fu,R. Dickinson,J. Joiner,C. Frankenberg,L. Gu,Y. Xia & N. Fernando (2015) Drought onset mechanisms revealed by satellite solar-induced chlorophyll fluorescence: Insights from two contrasting extreme events. *Journal of Geophysical Research: Biogeosciences,* 120, 2427-2440.

Swaminathan, M. S. & R. V. Bhavani (2013) Food production & availability - Essential prerequisites for sustainable food security. *The Indian Journal of Medical Research*, 138, 383-391.

Tilman, D.,C. Balzer,J. Hill & B. L. Befort (2011) Global food demand and the sustainable intensification of agriculture. *Proceedings of the National Academy of Sciences*, 108, 20260-20264.

TYAGI, S.,R. SINGH,P. KRISHNAN & R. VERMA (2013) Variations in Meteorological Conditions Resulted Decline in Wheat Yield in North-West Indo-Gangetic Plains. *Journal of Agricultural Physics*, 13, 175-181.

Verhulst, N.,B. Govaerts,V. Nelissen,K. D. Sayre,J. Crossa,D. Raes & J. Deckers (2011) The effect of tillage, crop rotation and residue management on maize and wheat growth and development evaluated with an optical sensor. *Field Crops Research*, 120, 58-67.

Verma, M.,D. Schimel,B. Evans,C. Frankenberg,J. Beringer,D. T. Drewry,T. Magney,I. Marang,L. Hutley & C. Moore (2017) Effect of environmental conditions on the relationship between solar-induced fluorescence and gross primary productivity at an OzFlux grassland site. *Journal of Geophysical Research: Biogeosciences*, 122, 716-733.

Wagle, P.,Y. Zhang,C. Jin & X. Xiao (2015) Comparison of solar-induced chlorophyll fluorescence, light-use efficiency, and process-based GPP models in maize. *Ecological Applications*.

Wang, J.,P. M. Rich & K. P. Price (2003) Temporal responses of NDVI to precipitation and temperature in the central Great Plains, USA. *International journal of remote sensing*, 24, 2345-2364.

Wang, X.,P. Ciais,L. Li,F. Ruget,N. Vuichard,N. Viovy,F. Zhou,J. Chang,X. Wu,H. Zhao & S. Piao (2017) Management outweighs climate change on affecting length of rice growing period for early rice and single rice in China during 1991–2012. *Agricultural and Forest Meteorology*, 233, 1-11.

Wardlaw, I. F. (1994) The effect of high temperature on kernel development in wheat: variability related to pre-heading and post-anthesis conditions. *Functional Plant Biology*, 21, 731-739.

White, J. W. 2003. Modeling temperature response in wheat and maize. CIMMYT.

Xie, Y.,P. Wang,X. Bai,J. Khan,S. Zhang,L. Li & L. Wang (2017) Assimilation of the leaf area index and vegetation temperature condition index for winter wheat yield estimation using

Landsat imagery and the CERES-Wheat model. *Agricultural and Forest Meteorology,* 246, 194-206.

Yoshida, Y.,J. Joiner,C. Tucker,J. Berry,J. E. Lee,G. Walker,R. Reichle,R. Koster,A. Lyapustin & Y. Wang (2015) The 2010 Russian drought impact on satellite measurements of solar-induced chlorophyll fluorescence: Insights from modeling and comparisons with parameters derived from satellite reflectances. *Remote Sensing of Environment,* 166, 163-177.

You, L. & S. Wood (2006) An entropy approach to spatial disaggregation of agricultural production. *Agricultural Systems,* 90, 329-347.

You, L.,S. Wood,U. Wood-Sichra & W. Wu (2014) Generating global crop distribution maps: From census to grid. *Agricultural Systems,* 127, 53-60.

Zhang, Y.,L. Guanter,J. A. Berry,J. Joiner,C. van der Tol,A. Huete,A. Gitelson,M. Voigt & P. Köhler (2014) Estimation of vegetation photosynthetic capacity from space-based measurements of chlorophyll fluorescence for terrestrial biosphere models. *Global Change Biology,* 20, 3727-3742.

Zhao, C.,B. Liu,S. Piao,X. Wang,D. B. Lobell,Y. Huang,M. Huang,Y. Yao,S. Bassu & P. Ciais (2017) Temperature increase reduces global yields of major crops in four independent estimates. *Proceedings of the National Academy of Sciences,* 114, 9326-9331.

**Supporting information**

*Vapor pressure deficit calculation*

Equations (1-3) below are employed to calculate the vapor pressure deficit (VPD):

$$\mathrm{VPD} = VP_{sat} - VP_{air} \quad (1)$$

Where $VP_{sat}$ is the saturation vapor pressure of the air in psi that is calculated using equation (2), $VP_{air}$ is the vapor pressure in the air in psi at the actual relative humidity that is calculated using equation (3).

$$VP_{sat} = e^{\frac{A}{T}+B+CT+DT^2+ET^3+F\times\ln(T)} \quad (2)$$

where T is the temperature of the air in Rankine, here we used the monthly ERA interim skin temperature with a spatial resolution of 0.5×0.5 degree as the input. $\mathrm{A} = -1.044 \times 10^4, B = -11.29, C = -2.7 \times 10^{-2}, D = 1.28910^{-5}, E = -2.478 \times 10^{-9}, F = 6.456$.

$$VP_{air} = VP_{sat} \times RH \div 100 \quad (3)$$

where RH is the relative humidity (%) of the air, the monthly ERA interim relative humidity with a spatial resolution of 0.5×0.5 degree was employed in this study.

*Wheat phenology calculation*

The phenology of the wheat in the study area was calculated by fitting double logistic functions to the GOME-2 SIF and AVHRR NDVI time series over the entire study area using Timesat software. The green-up date of each year was defined as the point when the fitted curves reached 10% of the maximum amplitude, and senescence was defined as the point when the fitted curves declined to 10% of the maximum for that year. The green season length (GSL) was calculated as the number of days between the green-up date and senescence (Jönsson and Eklundh 2004, Lobell, Sibley and Ivan Ortiz-Monasterio 2012).

Guan, K., J. A. Berry, Y. Zhang, J. Joiner, L. Guanter, G. Badgley & D. B. Lobell (2015) Improving the monitoring of crop productivity using spaceborne solar-induced fluorescence. *Global change biology*, 22**,** 716-726.

Jönsson, P. & L. Eklundh (2004) TIMESAT—a program for analyzing time-series of satellite sensor data. *Computers & Geosciences,* 30**,** 833-845.

Lobell, D., J. Hicke, G. Asner, C. Field, C. Tucker & S. Los (2002) Satellite estimates of productivity and light use efficiency in United States agriculture, 1982–98. *Global Change Biology,* 8**,** 722-735.

Lobell, D. B., A. Sibley & J. Ivan Ortiz-Monasterio (2012) Extreme heat effects on wheat senescence in India. *Nature Clim. Change,* 2**,** 186-189.

You, L., S. Wood, U. Wood-Sichra & W. Wu (2014) Generating global crop distribution maps: From census to grid. *Agricultural Systems,* 127**,** 53-60.

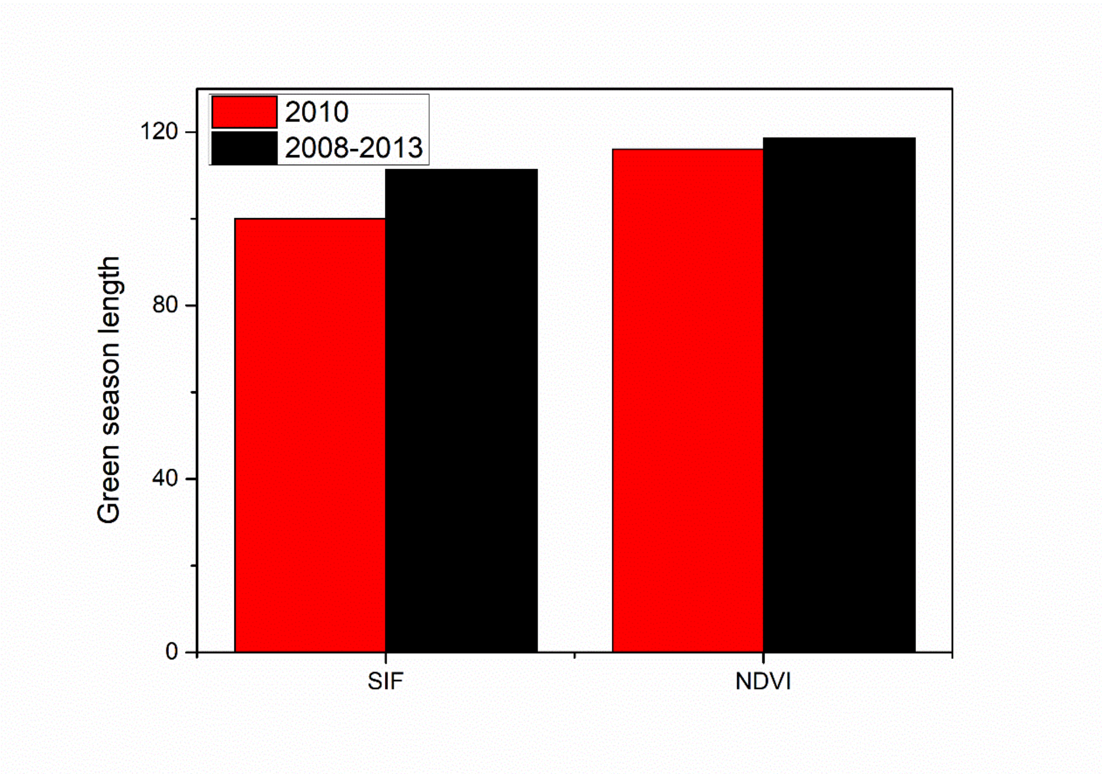


Figure S1. The growing season length (GSL) of wheat in the study area calculated by SIF and NDVI, the red bar indicates the GSL of 2010, and the black bar indicates the GSL value of the multiyear mean from 2008 to 2013.

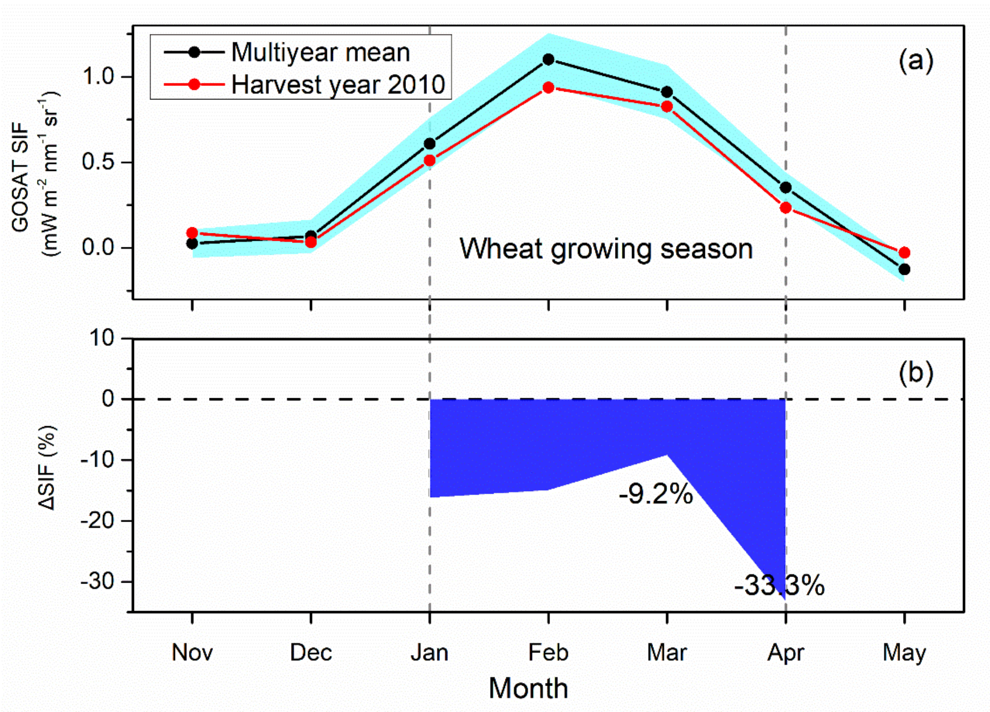


Figure S2. Seasonal variations of (a) the monthly and the entire study area means of the GOSAT SIF from November 2009 to May 2010 and (b) its change percent during the wheat growing season

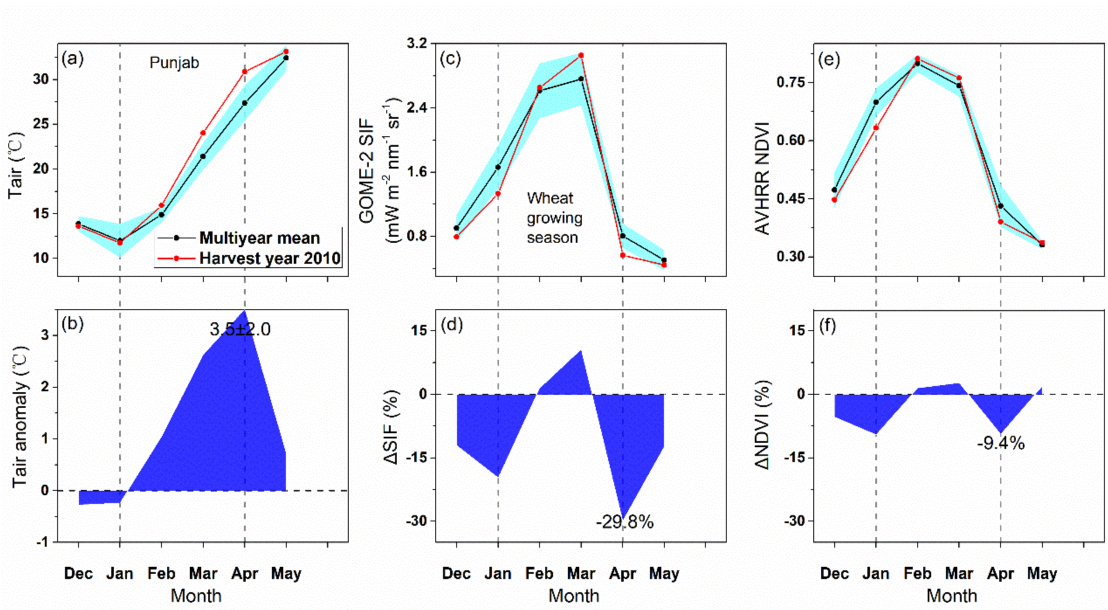

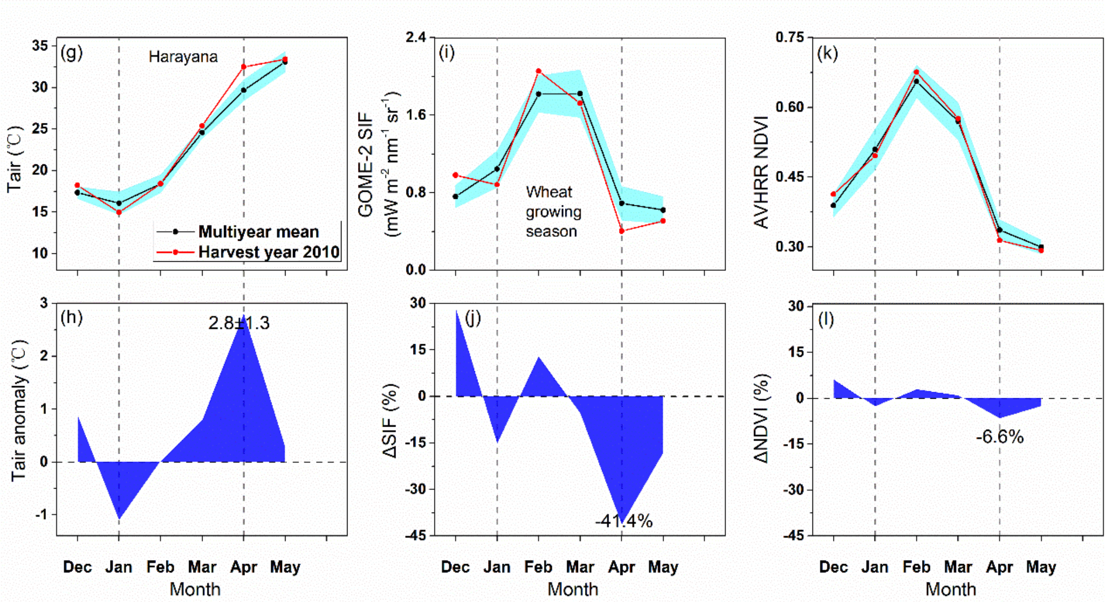


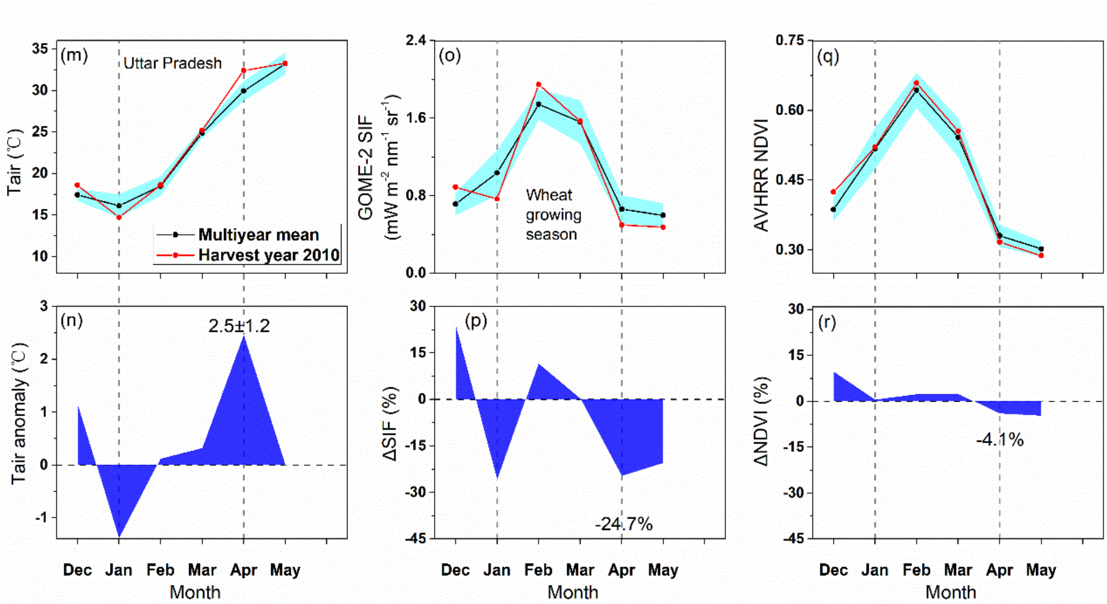


Figure S3. The monthly seasonal variations and the means of temperature (Tair) and their anomalies, GOME-2 SIF data, AVHRR NDVI data and their percent changes from December 2009 to May 2010 in three independent states (Punjab: a-f, Haryana: g-l and Uttar Pradesh: m-r)

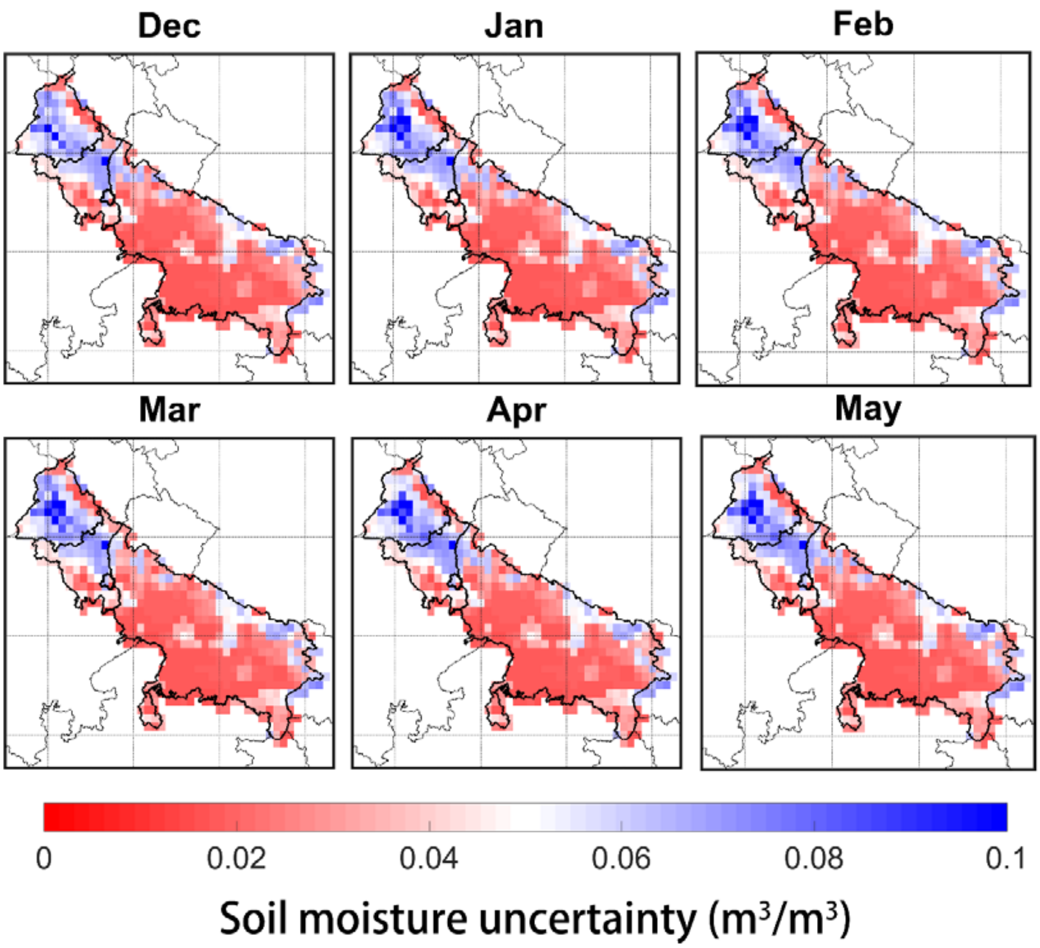


Figure S4 Spatial distributions of the ESA CCI soil moisture uncertainty from December 2009 to May 2010

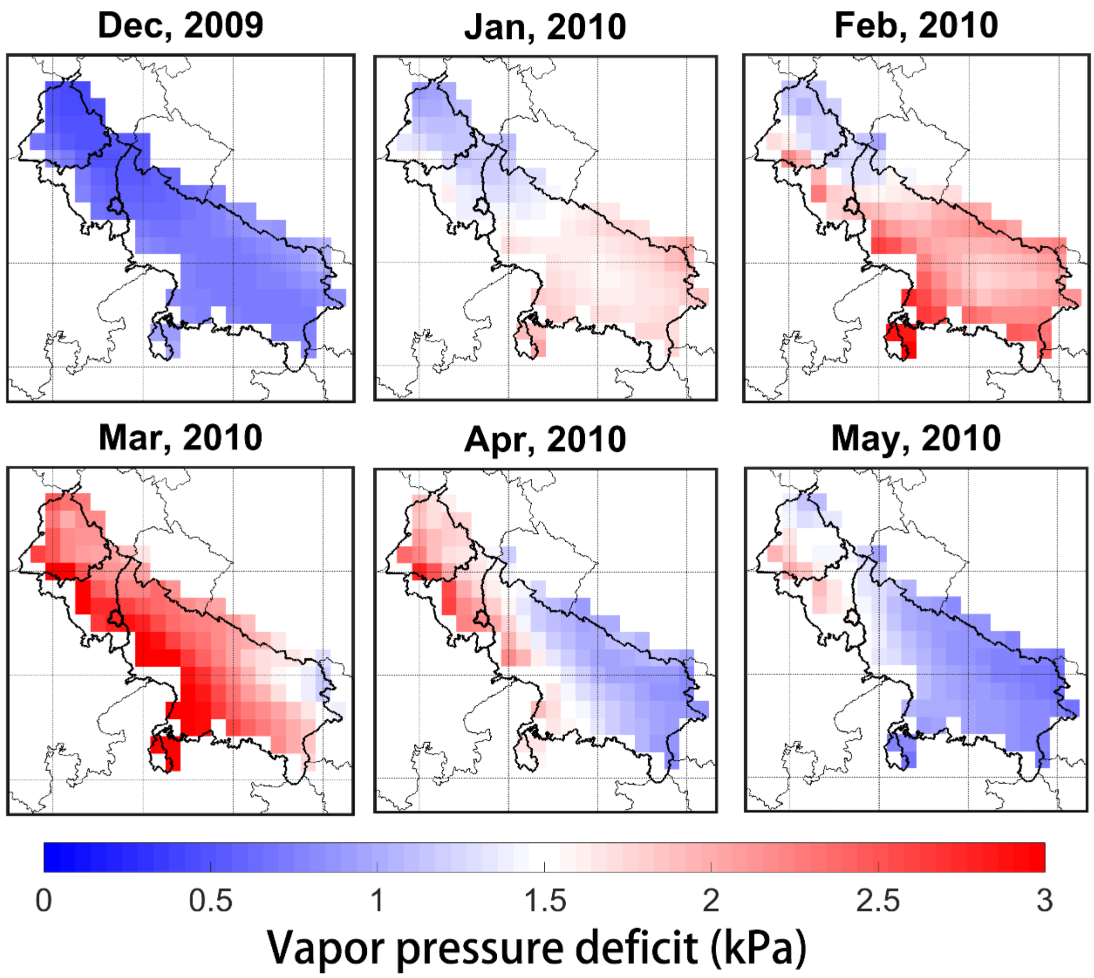


Figure S5. Spatial distributions of the absolute value of the Vapor pressure deficit (VPD) from December 2009 to May 2010

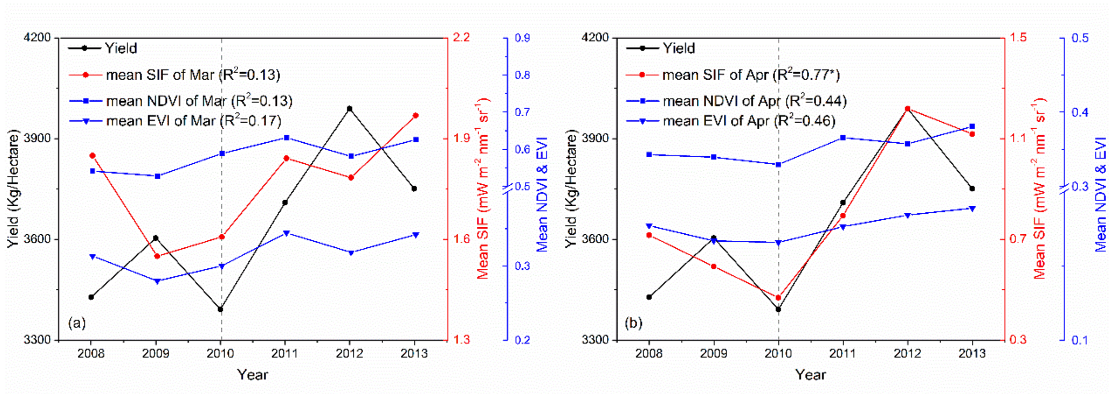


Figure S6. Inter-annual variations of yield and SIF/NDVI/EVI of March (a) and April (b) from 2008 to 2013 in the IGP area, the values of $R^2$ indicate the linear fit between SIF/NDVI/EVI and yield. Single asterisk (*) denote statistical significance levels of p-value <0.05.

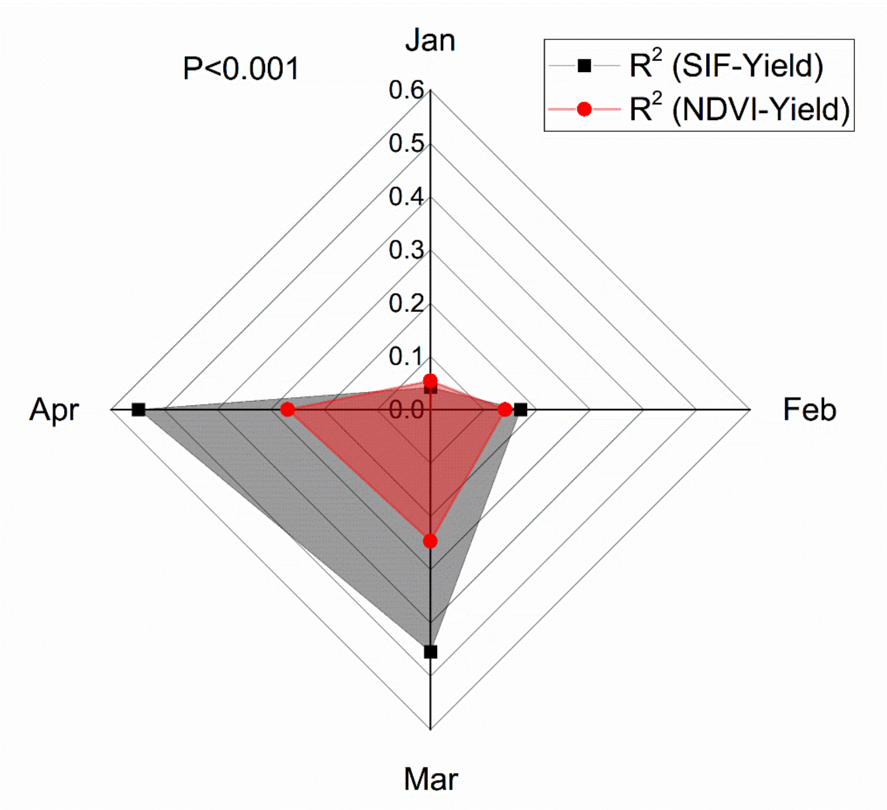


Figure S7. The determination coefficients ($R^2$) between yield and SIF/NDVI of January/February/March/April from 2008 to 2013 at county scale, all the linear correlations are statistical significant at levels of p-value<0.001.

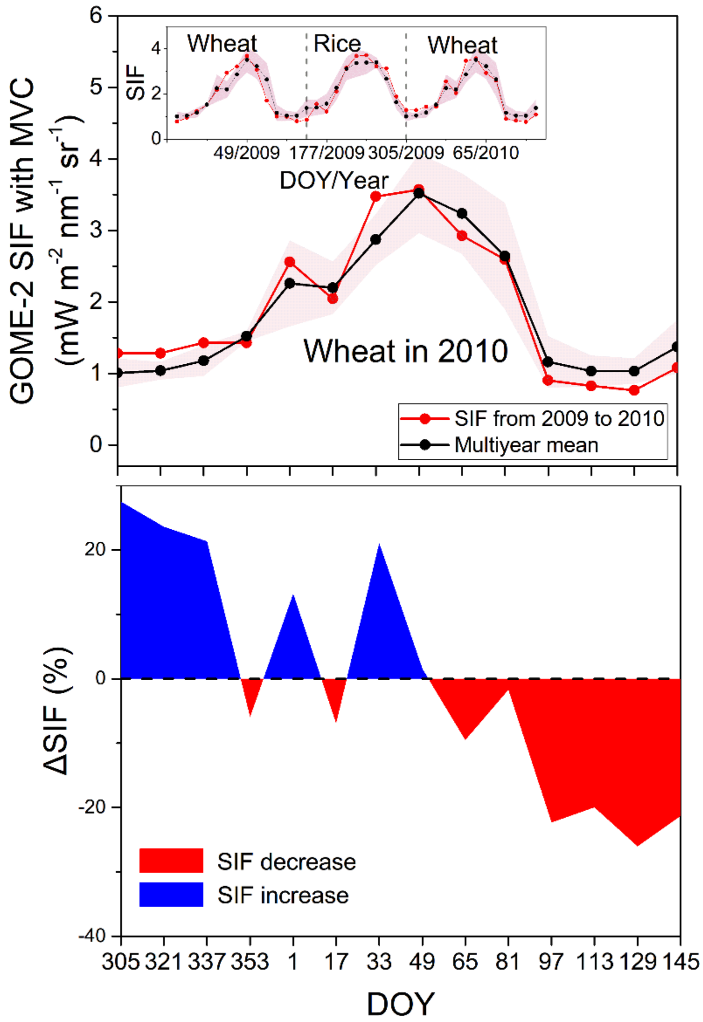


Figure S8. Seasonal variations of the 16-day maximum value compositing (MVC) of GOME-2 SIF, its multiyear mean and SIF change percent from December 2009 to May 2010.

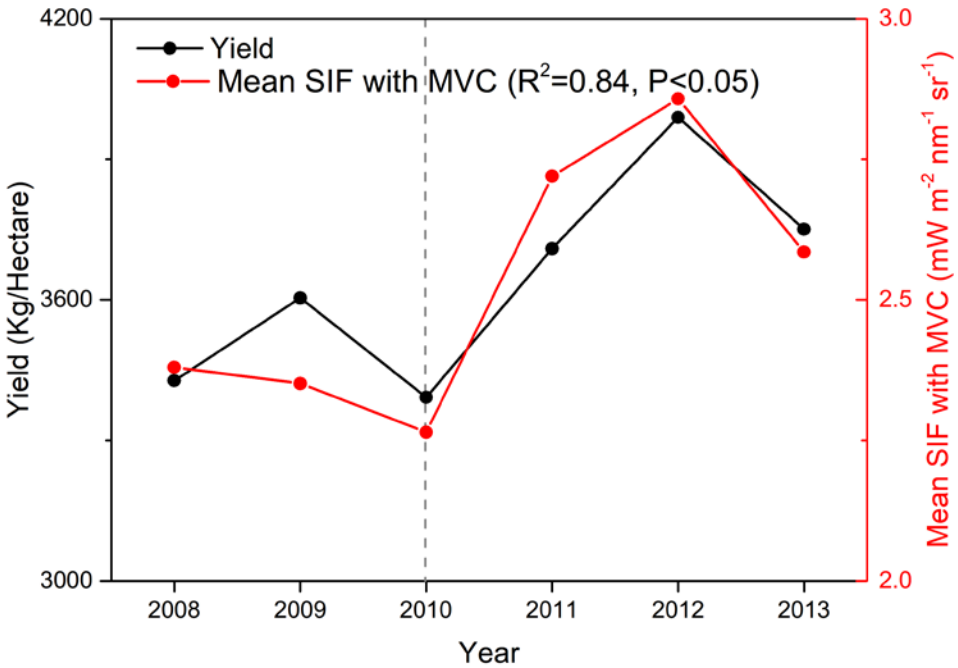


Figure S9. Interannual variations of yield and wheat growing season mean SIF with maximum value composite (MVC) processing from 2008 to 2013 in the IGP study area, the value of $R^2$ and P indicate the linear fit between $SIF_{MVC}$ and yield.